

# Valence quark distribution of light $\rho$ and heavy $J/\psi$ vector mesons in light-cone quark model

Tanisha<sup>1,\*</sup> Satyajit Puan<sup>1,†</sup> Anurag Yadav<sup>1,‡</sup> and Harleen Dahiya<sup>1§</sup>

<sup>1</sup> *Computational High Energy Physics Lab, Department of Physics,  
Dr. B.R. Ambedkar National Institute of Technology, Jalandhar, 144008, India*

(Dated: June 13, 2025)

arXiv:2505.09213v1 [hep-ph] 14 May 2025

## Abstract

In this work, we have investigated the valence quark structure of light  $\rho$  and heavy  $J/\psi$  vector mesons using the light-cone quark model through unpolarized quark generalized parton distributions (GPDs). By solving the quark-quark correlator, we have represented the quark GPDs in the form of light-front wave function (LFWFs). The charge, magnetic, and quadrupole form factors of these particles have been derived from the unpolarized quark GPDs and compared with the available theoretical predictions and lattice simulation data. The structure functions corresponding to the Rosenbluth scattering cross section of these mesons have also been calculated and compared with the available NJL model predictions. The results of our calculations are found to follow a similar trend as the other model results. We have also calculated the parton distribution functions (PDFs) of these particles in the forward limit of GPDs. The calculated PDFs have also been evolved to  $5 \text{ GeV}^2$  through next to next leading order Dokshitzer–Gribov–Lipatov–Altarelli–Parisi (DGLAP) evolutions.

*Keywords:* light and heavy vector mesons, generalized parton distributions (GPDs), parton distribution functions (PDFs), form factors (form factors), structure functions, light-cone quark model.

## I. INTRODUCTION

Vector mesons such as  $\rho$  and  $J/\psi$  play an important role in advancing our understanding of the Standard Model by offering a versatile testing ground for both the theoretical and experimental techniques. Owing to their differing mass scales and spin-1 character, they enable the exploration of polarization-sensitive effects and tensor structures that are not present in scalar or spin-1/2 systems. As such, these mesons provide a valuable context for assessing the applicability of effective models in describing hadronic phenomena across a wide range of energy scales. At the low energy scale  $\mu^2 \leq 1 \text{ GeV}^2$ , the valence quark contribution is more compared to gluons than at the high energy scale  $\mu^2 \geq 1 \text{ GeV}^2$  which is primarily due to confinement. Therefore, it becomes interesting to explore the valence quark behavior within the low energy quark models such as Nambu–Jona-Lasinio model (NJL) [1–3], light-front quark models (LFQM) [4–6], light-front holographic model (LFHM) [7, 8], spectator model [9, 10], quark-diquark model [11, 12], MIT-Bag model [13, 14],

---

\* tanisha220902@gmail.com

† puhansatyajit@gmail.com

‡ anuragyadav1431905@gmail.com

§ dahiyah@nitj.ac.in

contact interaction [15, 16], lattice simulations [17–19], etc.

Using these models, one can understand the internal structure of a hadron through the five-dimensional generalized transverse momentum distributions (GTMDs) [20–23], three-dimensional generalized parton distribution functions (GPDs) [24–27], transverse momentum parton distribution functions (TMDs) [28–31], one-dimensional parton distribution functions (PDFs) [32–34], etc. The transverse and spatial structure of the valence quark inside a hadron can be studied using the TMDs and GPDs. TMDs carry information about the transverse structure of the hadron in the form of transverse ( $\mathbf{k}_\perp$ ) and longitudinal ( $x$ ) momentum of the constituents with no information about the spatial structure, which can be accessed through GPDs as a functions of momentum transferred between final and initial state ( $\Delta_\perp$ ), longitudinal momentum ( $x$ ) and skewness parameter ( $\xi$ ). Elastic form factors (Eform factors), orbital angular momentum, charge radii, pressure and shear distributions, gravitational form factors, single spin asymmetry, etc of hadrons can be accessed through the GPDs [24, 35, 36]. GPDs can be extracted directly from deeply virtual Compton scattering (DVCS) [37, 38] and deeply virtual meson production (DVMP) [39]. TMDs and GPDs are the extended form of one-dimensional PDFs, which carry information about the longitudinal momentum fraction  $x$  carried by the constituent from the hadrons. PDFs can be extracted experimentally from the deep inelastic scattering process (DIS) [40]. One major issue in hadron physics has been and still is the lack of accurate information about the shapes of the above distribution functions generated from the first principle of quantum chromodynamics (QCD).

In this work, we have calculated the quark GPDs of spin-1 vector mesons within the light-cone quark model (LCQM) [41–43] as they have higher spin degrees of freedom and more polarizations as compared to spin-1/2 nucleons and spin-0 mesons. These polarizations occur due to the transverse and longitudinal polarizations of spin projections, resulting in the formation of tensor structures of spin-1 mesons. There are a total of nine GPDs present at the leading twist compared to eight of spin-1/2 nucleons and two of spin-0 mesons [44]. Out of nine quark GPDs, five are unpolarized and four are polarized quark GPDs for spin-1 vector mesons. In the present work, we have limited our work to compute the unpolarized quark GPDs only. However, polarized quark GPDs have been studied in NJL model [45] and LFQM [46] previously. These quark GPDs have been calculated at zero skewness from the quark-quark correlator and have been presented in the overlap form of light-front wave functions (LFWFs). It is established that the LFWF is Lorentz-invariant and can be represented in terms of the constituents' momentum fractions, which are unaffected by the overall hadron momentum. Thus, it is quite advantageous to learn how to derive

LFWFs from a fundamental standpoint and are essential for our knowledge of the hadron structure and the light-front quantization approach to QCD.

For the numerical calculations, we have considered both the light  $\rho$  and heavy  $J/\psi$  vector mesons. Out of five  $H_i(x, 0, -\Delta_\perp^2)$  ( $i = 1, \dots, 5$ ) GPDs,  $H_4(x, 0, -\Delta_\perp^2)$  comes out to be zero,  $H_1$  gives rise to the  $F_1(x)$  structure function of the DIS process and  $H_5$  carries information about the polarized  $b_1(x)$  structure function of the spin-1 mesons. The quark GPDs of vector mesons have been studied in different theoretical models [45, 47–51] whereas till now there are no lattice simulations and experimental results available. A total of three form factors are present for the leading twist unpolarized GPDs case: charge ( $G_c$ ), magnetic ( $G_M$ ), and quadrupole ( $G_Q$ ) form factors [52]. These form factors encode information about the charge radii, magnetic moment, and quadrupole moment of the mesons. These form factors can be used to calculate the structure functions corresponding to the Rosenbluth cross section [53]. There has been a wide range of theoretical studies reported for these form factors [45, 47–51, 54–59] and few lattice simulation studies [60, 61]. However, there has been a complete lack of experimental studies for both the particles. Further, for the sake of completeness, we have also predicted the quark PDFs for both the particles. There are a total of four PDFs present at the leading twist for spin-1 mesons compared to one for spin-0 mesons and three for spin-1/2 nucleons [62]. These are unpolarized  $f_1(x)$ , transversity  $h_1(x)$ , helicity  $g_1(x)$ , and tensor  $f_{1LL}$  quark PDFs. The unpolarized  $f_1(x)$  and tensor polarized  $f_{1LL}(x)$  quark PDFs can be derived from  $H_1$  and  $H_5$  quark GPDs at the forward limit  $\Delta_\perp = 0$ . However, the  $f_{1LL}$  PDF is found to be zero for our case. For numerical calculations, we have adopted the LCQM with Brodsky-Huang-Leepage (BHL) prescription for the momentum space wave function [63] and spin wave functions through Melosh-Wigner rotation [42, 64].

The paper is arranged as follows. In Sec. II, we have discussed the LCQM along with the spin and momentum wave function in light-front (LF) formalism. The derivation and discussion of unpolarized quark GPDs from quark-quark correlator has been presented in Sec. III. In this section, we have also derived and discussed the different form factors along with structure functions. In Sec. IV, we have presented the quark parton distribution functions for spin-1 vector mesons. We have finally summarized our work in Sec. V.

## II. METHODOLOGY

### A. Light-cone quark model

Understanding hadrons as relativistic bound states of partons is a central goal of modern particle physics. The LF formalism provides an elegant approach to this problem, expressing the hadron's wave function as a sum over Fock-states defined by the momentum and spin of its constituents. The hadron wave function based on LF quantization QCD using the multi-particle Fock-state expansion is expressed as [41–43]

$$|M_h(P, S_z)\rangle = \sum_{n, \lambda_j} \int \prod_{j=1}^n \frac{dx_j d^2\mathbf{k}_{\perp j}}{\sqrt{x_j} 16\pi^3} 16\pi^3 \delta\left(1 - \sum_{j=1}^n x_j\right) \delta^{(2)}\left(\sum_{j=1}^n \mathbf{k}_{\perp j}\right) \psi_{n/M}(x_j, \mathbf{k}_{\perp j}, \lambda_j) |n; \mathbf{k}_j^+, \mathbf{k}_{\perp j}, \lambda_j\rangle.$$

Here,  $|M_h(P, S_z)\rangle$  is the hadron eigenstate with  $P = (P^+, P^-, P_\perp)$  and  $S_z$  being the hadron's total average momentum and longitudinal spin projection, respectively.  $n$  is the number of constituents inside the hadron,  $\lambda_j$  is the helicity of the  $j$ -th constituent of the hadron,  $\mathbf{k}_j = (\mathbf{k}_j^+, \mathbf{k}_j^-, \mathbf{k}_{j\perp})$  is the momentum of the  $j$ -th constituent of the hadron and  $x_j = P^+/\mathbf{k}_j^+$  is the longitudinal momentum fraction carried by the  $j$ -th constituent from the hadron. Both longitudinal momentum fraction and transverse momenta of the constituents of the hadron obey the momentum sum rule

$$\sum_{j=1}^n \mathbf{k}_j = 0, \quad \sum_{j=1}^n x_j = 1. \quad (1)$$

As we are dealing with mesons in this work, the meson Fock-state can be written in terms of quarks, gluons, and sea-quark degrees of freedom as [63, 65, 66]

$$|M\rangle = \sum |q\bar{q}\rangle\psi_{q\bar{q}} + \sum |q\bar{q}g\rangle\psi_{q\bar{q}g} + \sum |q\bar{q}gg\rangle\psi_{q\bar{q}gg} + |q\bar{q}(q\bar{q})_{sea}\rangle\psi_{q\bar{q}(q\bar{q})_{sea}} + \cdots, \quad (2)$$

where  $|M\rangle$  denotes the meson eigenstate. Since the higher Fock-state contribution is very less compared to  $|q\bar{q}\rangle$  leading state for the case of heavy mesons [67], we have not considered the higher Fock-state contribution in this work. The two-particle meson minimal Fock-state can be written in terms of the intrinsic momenta of the quark and antiquark from Eq. (1) as

$$|M(P, S_z)\rangle = \sum_{\lambda_1, \lambda_2} \int \frac{dx d^2\mathbf{k}_\perp}{\sqrt{x(1-x)} 2(2\pi)^3} \Psi_{S_z}(x, \mathbf{k}_\perp, \lambda_1, \lambda_2) |x, \mathbf{k}_\perp, \lambda_1, \lambda_2\rangle. \quad (3)$$

Here,  $\lambda_{1(2)}$  are the helicities of quark (antiquark),  $\Psi_{S_z}(x, \mathbf{k}_\perp, \lambda_1, \lambda_2)$  is the LF meson wave function with different spin ( $S_z$ ) and quark (antiquark) helicity ( $\lambda$ ) projections.  $x$  and  $1-x$  are the momentum fractions carried by the active quark and antiquark, respectively. The LF meson wave function

can be expressed as

$$\Psi_{S_z}(x, \mathbf{k}_\perp, \lambda_1, \lambda_2) = \mathcal{S}_{S_z}(x, \mathbf{k}_\perp, \lambda_1, \lambda_2) \psi_{q\bar{q}}(x, \mathbf{k}_\perp). \quad (4)$$

Here,  $\mathcal{S}_{S_z}(x, \mathbf{k}_\perp, \lambda_1, \lambda_2)$  and  $\psi_{q\bar{q}}(x, \mathbf{k}_\perp)$  are the spin and momentum space wave functions of the mesons respectively. By adopting the Brodsky-Huang-Lepage (BHL) prescription, the momentum space wave function in Eq. (4) can be expressed as [42, 68]

$$\psi_{q\bar{q}}(x, \mathbf{k}_\perp) = A \exp \left[ - \frac{\frac{\mathbf{k}_\perp^2 + m_q^2}{x} + \frac{\mathbf{k}_\perp^2 + m_{\bar{q}}^2}{1-x}}{8\beta^2} \right], \quad (5)$$

where  $m_q$  and  $m_{\bar{q}}$  are the quark and antiquark masses respectively.  $\beta$  and  $A$  are the harmonic scale parameter and normalization constant of the meson. The quark masses ( $m_{q(\bar{q})}$ ) and  $\beta$  are calculated by fitting with the mass spectra and decay constant of the respective mesons. For this work, we have adopted the quark mass  $m_{u(\bar{d})} = 0.2$  GeV and  $m_{c\bar{c}} = 1.68$  GeV for light  $\rho(u\bar{d})$  [69] and heavy  $J/\psi(c\bar{c})$  vector mesons [31], respectively. The  $\beta$  parameter is taken to be 0.410 and 0.699 for  $\rho(u\bar{d})$  and  $J/\psi(c\bar{c})$  vector mesons, respectively [31, 69]. The normalization constant is calculated by normalizing the momentum space wave function as

$$\int \frac{dx d^2\mathbf{k}_\perp}{2(2\pi)^3} |\psi_{q\bar{q}}(x, \mathbf{k}_\perp)|^2 = 1. \quad (6)$$

The four-vector momenta of the constituent quark ( $k_1$ ) and antiquark ( $k_2$ ) in the LF frame are respectively defined as

$$k_1 \equiv \left( xP^+, \frac{\mathbf{k}_\perp^2 + m_q^2}{xP^+}, \mathbf{k}_\perp \right), \quad (7)$$

$$k_2 \equiv \left( (1-x)P^+, \frac{\mathbf{k}_\perp^2 + m_{\bar{q}}^2}{(1-x)P^+}, -\mathbf{k}_\perp \right), \quad (8)$$

with  $M_{q\bar{q}}$  being the invariant mass of the composite meson system defined in terms of its quark mass  $m_q$  and antiquark mass  $m_{\bar{q}}$  as

$$M_{q\bar{q}}^2 = \frac{\mathbf{k}_\perp^2 + m_q^2}{x} + \frac{\mathbf{k}_\perp^2 + m_{\bar{q}}^2}{1-x}. \quad (9)$$

$\mathcal{S}_{S_z}(x, \mathbf{k}_\perp, \lambda_1, \lambda_2)$  in Eq. (5) is front-form spin wave function derived from the instant form by Melosh-Wigner rotation [42, 68, 70]. This transformation of instant form state  $\Phi(T)$  and front form state  $\Phi(F)$  is expressed as

$$\Phi_i^\uparrow(T) = - \frac{[\mathbf{k}_i^R \Phi_i^\downarrow(F) - (\mathbf{k}_i^+ + m_{q(\bar{q})}) \Phi_i^\uparrow(F)]}{\omega_{i(q\bar{q})}}, \quad (10)$$

$$\Phi_i^\downarrow(T) = \frac{[\mathbf{k}_i^L \Phi_i^\uparrow(F) + (\mathbf{k}_i^+ + m_{q(\bar{q})}) \Phi_i^\downarrow(F)]}{\omega_{i(q\bar{q})}}. \quad (11)$$

Here,  $\Phi(F)$  is a two-component Dirac spinor and  $\mathbf{k}_i^{R(L)} = \mathbf{k}_i^1 \pm \iota \mathbf{k}_i^2$ .  $\omega_{i(q\bar{q})}$  is defined as  $\omega_{i(q\bar{q})} = 1/\sqrt{2\mathbf{k}_i^+(\mathbf{k}^0 + m_{q(\bar{q})})}$ . Now applying different momenta forms from Eqs. (7)-(8) in Melosh-Wigner rotation, the spin wave function is obtained in the form of  $\kappa_{S_z}^F(x, \mathbf{k}_\perp, \lambda_1, \lambda_2)$  coefficient as

$$\mathcal{S}_{S_z}(x, \mathbf{k}_\perp, \lambda_1, \lambda_2) = \sum_{\lambda_1, \lambda_2} \kappa_{S_z}^F(x, \mathbf{k}_\perp, \lambda_1, \lambda_2) \Phi_1^{\lambda_1}(F) \Phi_2^{\lambda_2}(F). \quad (12)$$

These spin-wave function coefficients satisfy the following normalization relation

$$\sum_{\lambda_1, \lambda_2} \kappa_{S_z}^{F*}(x, \mathbf{k}_\perp, \lambda_1, \lambda_2) \kappa_{S_z}^F(x, \mathbf{k}_\perp, \lambda_1, \lambda_2) = 1. \quad (13)$$

Similarly, the same spin-wave function can be calculated using the proper vertex chosen for the vector meson [42, 64] as

$$\mathcal{S}_{S_z}(x, \mathbf{k}_\perp, \lambda_1, \lambda_2) = \bar{u}(k_1, \lambda_1) \left[ -\frac{1}{\sqrt{2} \sqrt{M_{q\bar{q}}^2 - (m_q - m_{\bar{q}})^2}} (\gamma^\mu - \frac{k_1^\mu - k_2^\mu}{M_{q\bar{q}} + m_q + m_{\bar{q}}}) \epsilon(P, S_z) \right] v(k_2, \lambda_2). \quad (14)$$

Here,  $u$  and  $v$  are the Dirac spinors. In this work, we have only considered the light  $\rho(u\bar{d})$  vector and heavy  $J/\psi(c\bar{c})$  vector mesons, so  $m_q = m_{\bar{q}}$  for this case.  $\epsilon(P, S_z)$  is the polarization vector of the vector mesons, which can be expressed for both transverse ( $S_z = \pm 1$ ) and longitudinal polarization ( $S_z = 0$ ) as

$$\begin{aligned} \epsilon(P, S_z = \pm 1) &= (\epsilon_{\pm 1}^+, \epsilon_{\pm 1}^-, \epsilon_{\pm 1}^\perp) = \left( 0, \frac{\mp \sqrt{2} P^{R,L}}{P^+}, \mp \frac{1}{\sqrt{2}}, -\frac{\iota}{\sqrt{2}} \right), \\ \epsilon(P, S_z = 0) &= (\epsilon_0^+, \epsilon_0^-, \epsilon_0^\perp) = \frac{1}{M_{q\bar{q}}} \left( P^+, \frac{P_\perp^2 - M_{q\bar{q}}^2}{P^+}, P_\perp \right). \end{aligned} \quad (15)$$

Here,  $P^{R,L} = P_1 \pm i P_2$ . Both the above methods give rise to the same form of spin wave function. The spin wave functions for vector mesons for different spin projections/polarization and different helicities of quark antiquark ( $\lambda = (\uparrow, \downarrow)$ ) are expressed for  $S_z = +1$  as [42]

$$\begin{aligned} \mathcal{S}_{(S_z=+1)}(x, \mathbf{k}_\perp, \uparrow, \uparrow) &= \frac{1}{\omega_{q\bar{q}}} [\mathbf{k}_\perp^2 + (M_{q\bar{q}} + m_q + m_{\bar{q}})((1-x)m_q + xm_{\bar{q}})], \\ \mathcal{S}_{(S_z=+1)}(x, \mathbf{k}_\perp, \uparrow, \downarrow) &= \frac{1}{\omega_{q\bar{q}}} [(\mathbf{k}_1 + \iota \mathbf{k}_2)(xM_{q\bar{q}} + m_q)], \\ \mathcal{S}_{(S_z=+1)}(x, \mathbf{k}_\perp, \downarrow, \uparrow) &= \frac{1}{\omega_{q\bar{q}}} [-(\mathbf{k}_1 + \iota \mathbf{k}_2)((1-x)M_{q\bar{q}} + m_{\bar{q}})], \\ \mathcal{S}_{(S_z=+1)}(x, \mathbf{k}_\perp, \downarrow, \downarrow) &= \frac{1}{\omega_{q\bar{q}}} [-(\mathbf{k}_1 + \iota \mathbf{k}_2)^2]. \end{aligned} \quad (16)$$

For longitudinal spin projection  $S_z=0$ , the spin wave functions are

$$\begin{aligned} \mathcal{S}_{(S_z=0)}(x, \mathbf{k}_\perp, \uparrow, \uparrow) &= \frac{1}{\sqrt{2}} \frac{1}{\omega_{q\bar{q}}} [(\mathbf{k}_1 - \iota \mathbf{k}_2)((1-2x)M_{q\bar{q}} + (m_{\bar{q}} - m_q))], \\ \mathcal{S}_{(S_z=0)}(x, \mathbf{k}_\perp, \uparrow, \downarrow) &= \frac{1}{\sqrt{2}} \frac{1}{\omega_{q\bar{q}}} [2\mathbf{k}_\perp^2 + (M_{q\bar{q}} + m_q + m_{\bar{q}})((1-x)m_q + xm_{\bar{q}})], \\ \mathcal{S}_{(S_z=0)}(x, \mathbf{k}_\perp, \downarrow, \uparrow) &= \frac{1}{\sqrt{2}} \frac{1}{\omega_{q\bar{q}}} [2\mathbf{k}_\perp^2 + (M_{q\bar{q}} + m_q + m_{\bar{q}})((1-x)m_q + xm_{\bar{q}})], \\ \mathcal{S}_{(S_z=0)}(x, \mathbf{k}_\perp, \downarrow, \downarrow) &= \frac{1}{\sqrt{2}} \frac{1}{\omega_{q\bar{q}}} [(-\mathbf{k}_1 - \iota \mathbf{k}_2)((1-2x)M_{q\bar{q}} + (m_{\bar{q}} - m_q))]. \end{aligned} \quad (17)$$

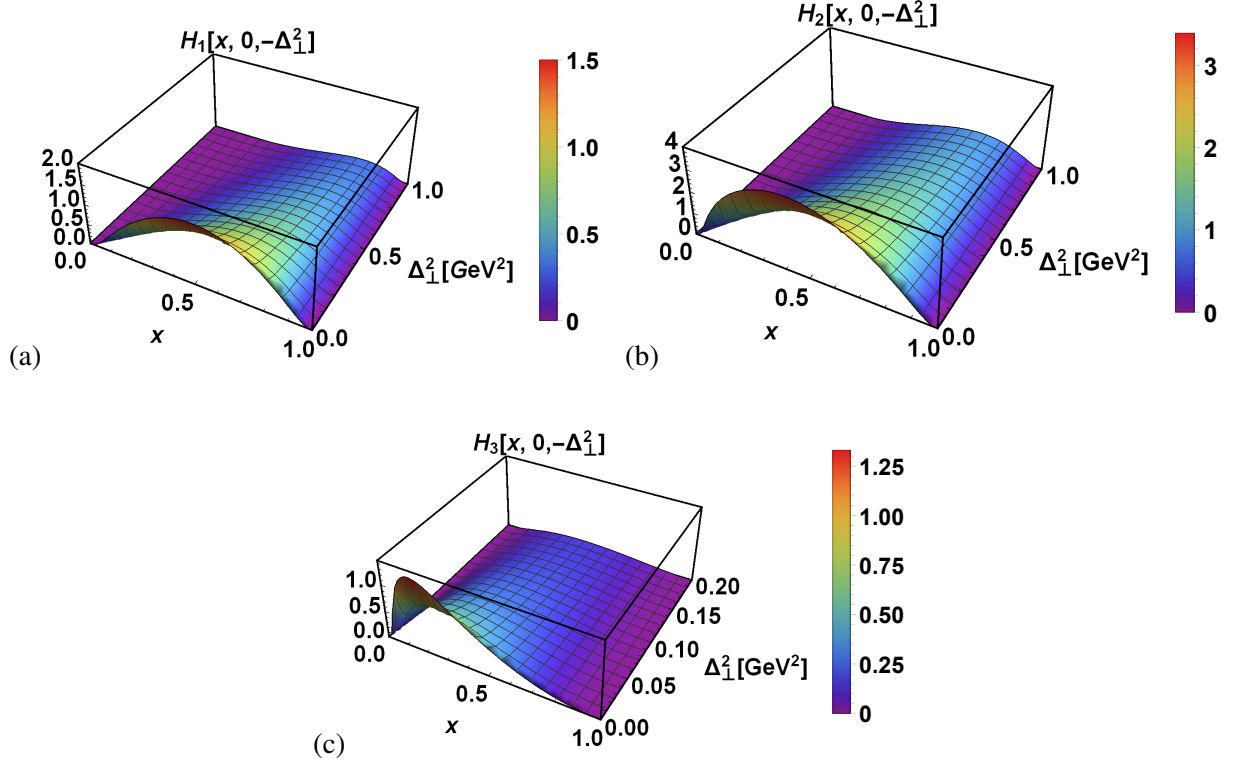


FIG. 1: (Color online) The three-dimensional quark GPDs have been plotted with respect to longitudinal momentum fraction ( $x$ ) and transverse momentum transferred  $\Delta_\perp^2$  ( $\text{GeV}^2$ ) for  $\rho$ -meson in (a) for  $H_1(x, 0, -\Delta_\perp^2)$ , (b) for  $H_2(x, 0, -\Delta_\perp^2)$ , and (c) for  $H_3(x, 0, -\Delta_\perp^2)$ .

Finally, the spin wave functions for transverse spin projection  $S_z = -1$  are

$$\begin{aligned}
\mathcal{S}_{(S_z=-1)}(x, \mathbf{k}_\perp, \uparrow, \uparrow) &= \frac{1}{\omega_{q\bar{q}}} [-(\mathbf{k}_1 - \mathbf{k}_2)^2], \\
\mathcal{S}_{(S_z=-1)}(x, \mathbf{k}_\perp, \uparrow, \downarrow) &= \frac{1}{\omega_{q\bar{q}}} [(\mathbf{k}_1 - \mathbf{k}_2)((1-x)M_{q\bar{q}} + m_{\bar{q}})], \\
\mathcal{S}_{(S_z=-1)}(x, \mathbf{k}_\perp, \downarrow, \uparrow) &= \frac{1}{\omega_{q\bar{q}}} [-(\mathbf{k}_1 - \mathbf{k}_2)(xM_{q\bar{q}} + m_q)], \\
\mathcal{S}_{(S_z=-1)}(x, \mathbf{k}_\perp, \downarrow, \downarrow) &= \frac{1}{\omega_{q\bar{q}}} [\mathbf{k}_\perp^2 + (M_{q\bar{q}} + m_q + m_{\bar{q}})((1-x)m_q + xm_{\bar{q}})].
\end{aligned} \tag{18}$$

Here,  $\omega_{q\bar{q}} = (M_{q\bar{q}} + m_q + m_{\bar{q}}) \sqrt{x(1-x)[M_{q\bar{q}}^2 - (m_q - m_{\bar{q}})^2]}$ . The two-particle Fock-state in Eq. (3) can be written in the form of LFWFs with all possible helicities of its constituent quark and antiquark for vector mesons as

$$\begin{aligned}
|M(P^+, \mathbf{P}_\perp, S_z)\rangle &= \int \frac{dx d^2\mathbf{k}_\perp}{2(2\pi)^3 \sqrt{x(1-x)}} [\Psi_{S_z}(x, \mathbf{k}_\perp, \uparrow, \uparrow) |xP^+, \mathbf{k}_\perp, \uparrow, \uparrow\rangle \\
&\quad + \Psi_{S_z}(x, \mathbf{k}_\perp, \downarrow, \downarrow) |xP^+, \mathbf{k}_\perp, \downarrow, \downarrow\rangle + \Psi_{S_z}(x, \mathbf{k}_\perp, \downarrow, \uparrow) \\
&\quad |xP^+, \mathbf{k}_\perp, \downarrow, \uparrow\rangle + \Psi_{S_z}(x, \mathbf{k}_\perp, \uparrow, \downarrow) |xP^+, \mathbf{k}_\perp, \uparrow, \downarrow\rangle].
\end{aligned} \tag{19}$$



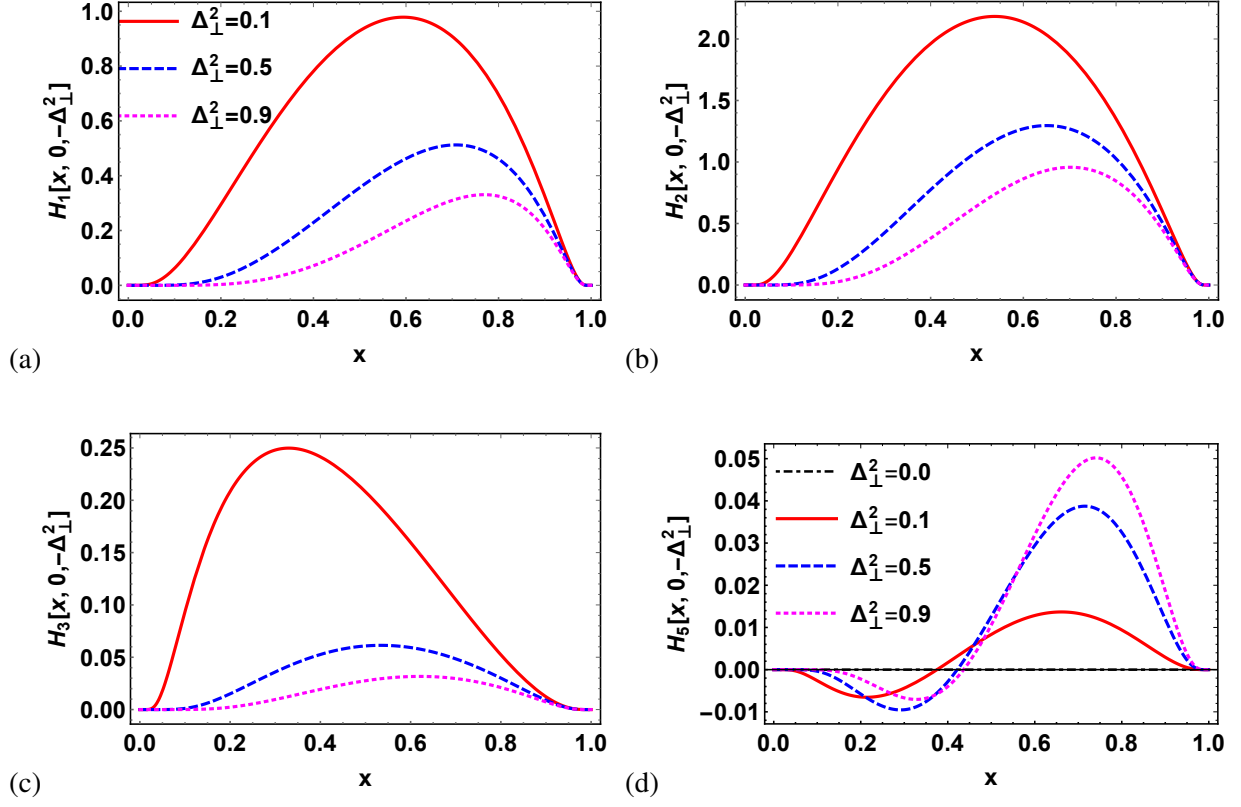


FIG. 2: (Color online) The quark GPDs of  $\rho$ -meson (a)  $H_1(x, 0, -\Delta_\perp^2)$ , (b)  $H_2(x, 0, -\Delta_\perp^2)$ , (c)  $H_3(x, 0, -\Delta_\perp^2)$ , and (d)  $H_5(x, 0, -\Delta_\perp^2)$  have been plotted with respect to longitudinal momentum fraction ( $x$ ) at fixed value of  $\Delta_\perp^2 = 0, 0.1, 0.2$  and  $0.9 \text{ GeV}^2$ .

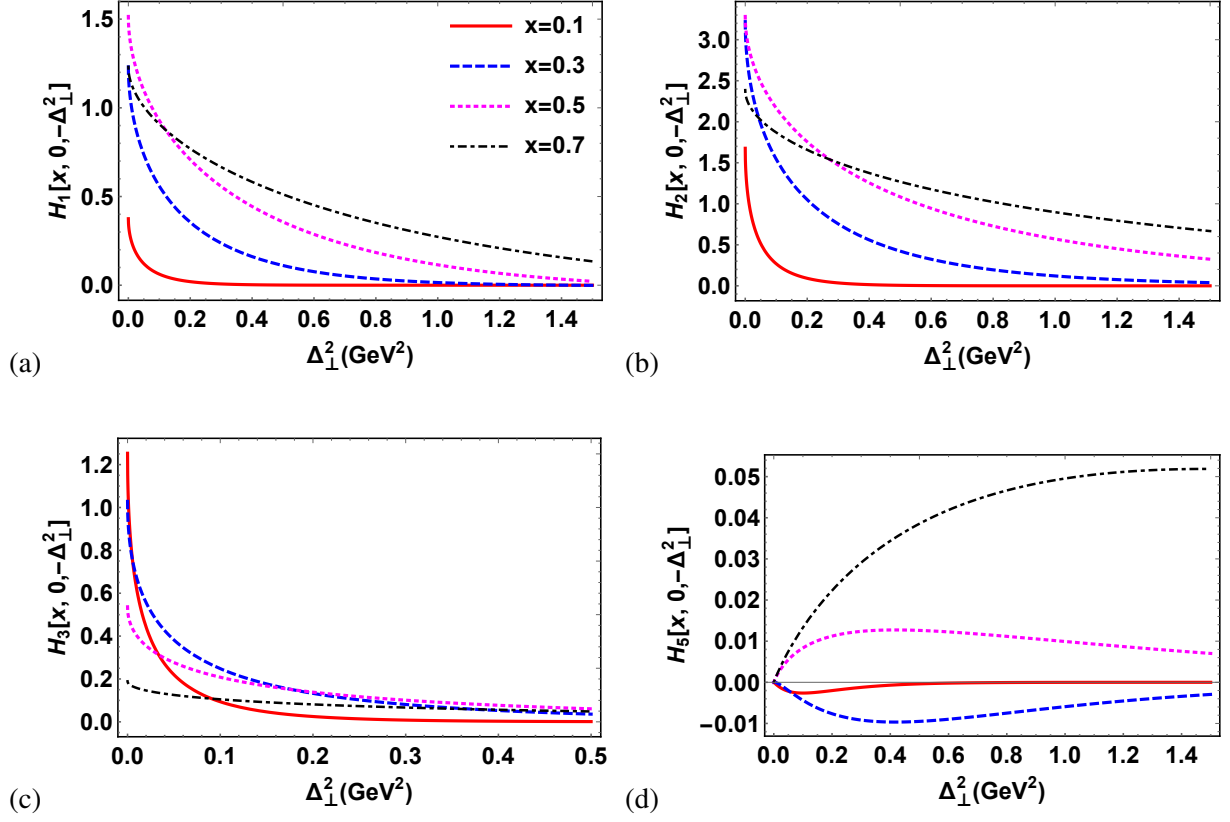


FIG. 3: (Color online) The quark GPDs of  $\rho$ -meson (a)  $H_1(x, 0, -\Delta_\perp^2)$ , (b)  $H_2(x, 0, -\Delta_\perp^2)$ , (c)  $H_3(x, 0, -\Delta_\perp^2)$ , and (d)  $H_5(x, 0, -\Delta_\perp^2)$  have been plotted with respect to  $\Delta_\perp^2$  at fixed value of longitudinal momentum fraction  $x = 0.1, 0.3, 0.5$  and  $0.7$ .

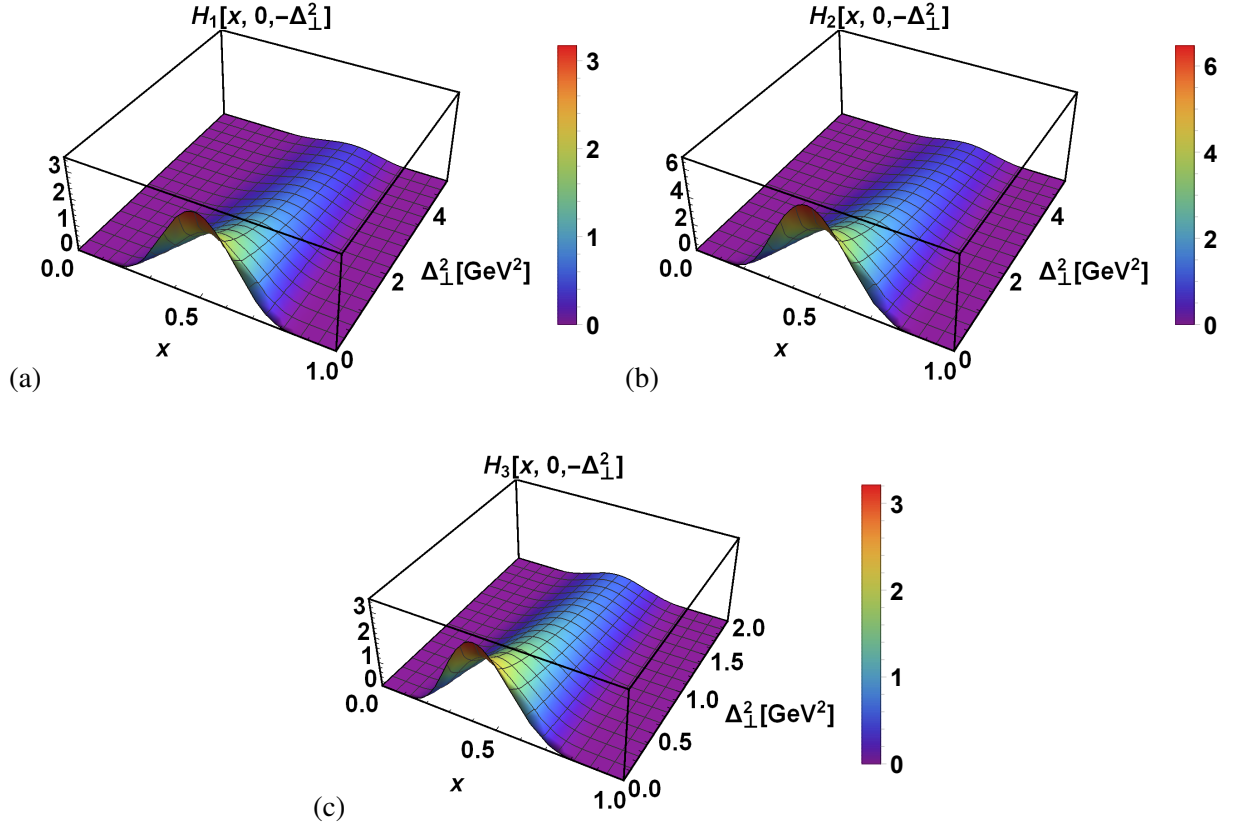


FIG. 4: (Color online) The three-dimensional quark GPDs have been plotted with respect to longitudinal momentum fraction ( $x$ ) and transverse momentum transferred  $\Delta_\perp^2$  ( $\text{GeV}^2$ ) for  $J/\psi$ -meson in (a) for  $H_1(x, 0, -\Delta_\perp^2)$ , (b) for  $H_2(x, 0, -\Delta_\perp^2)$ , and (c) for  $H_3(x, 0, -\Delta_\perp^2)$ .

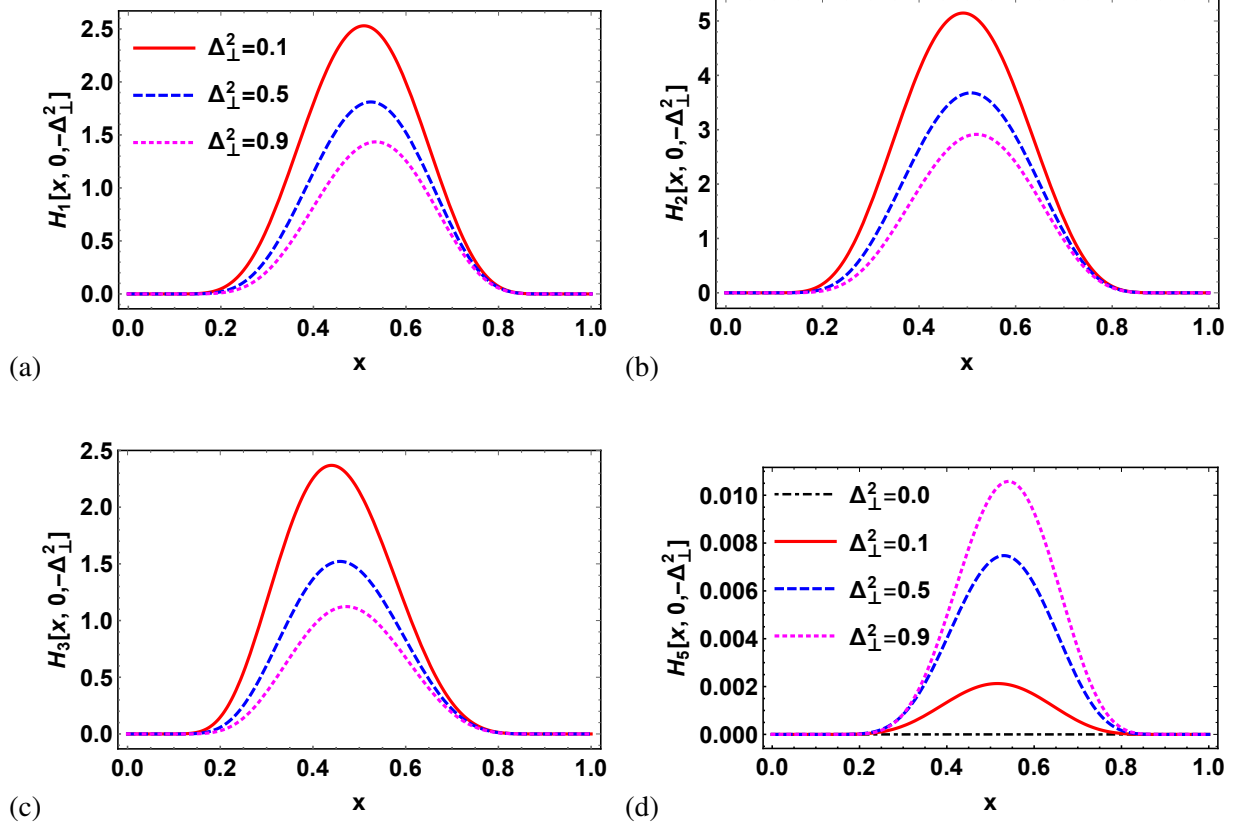


FIG. 5: (Color online) The quark GPDs of  $J/\psi$ -meson (a)  $H_1(x, 0, -\Delta_\perp^2)$ , (b)  $H_2(x, 0, -\Delta_\perp^2)$ , (c)  $H_3(x, 0, -\Delta_\perp^2)$ , and (d)  $H_5(x, 0, -\Delta_\perp^2)$  have been plotted with respect to longitudinal momentum fraction ( $x$ ) at fixed value of  $\Delta_\perp^2 = 0.1, 0.2$  and  $0.9 \text{ GeV}^2$ .

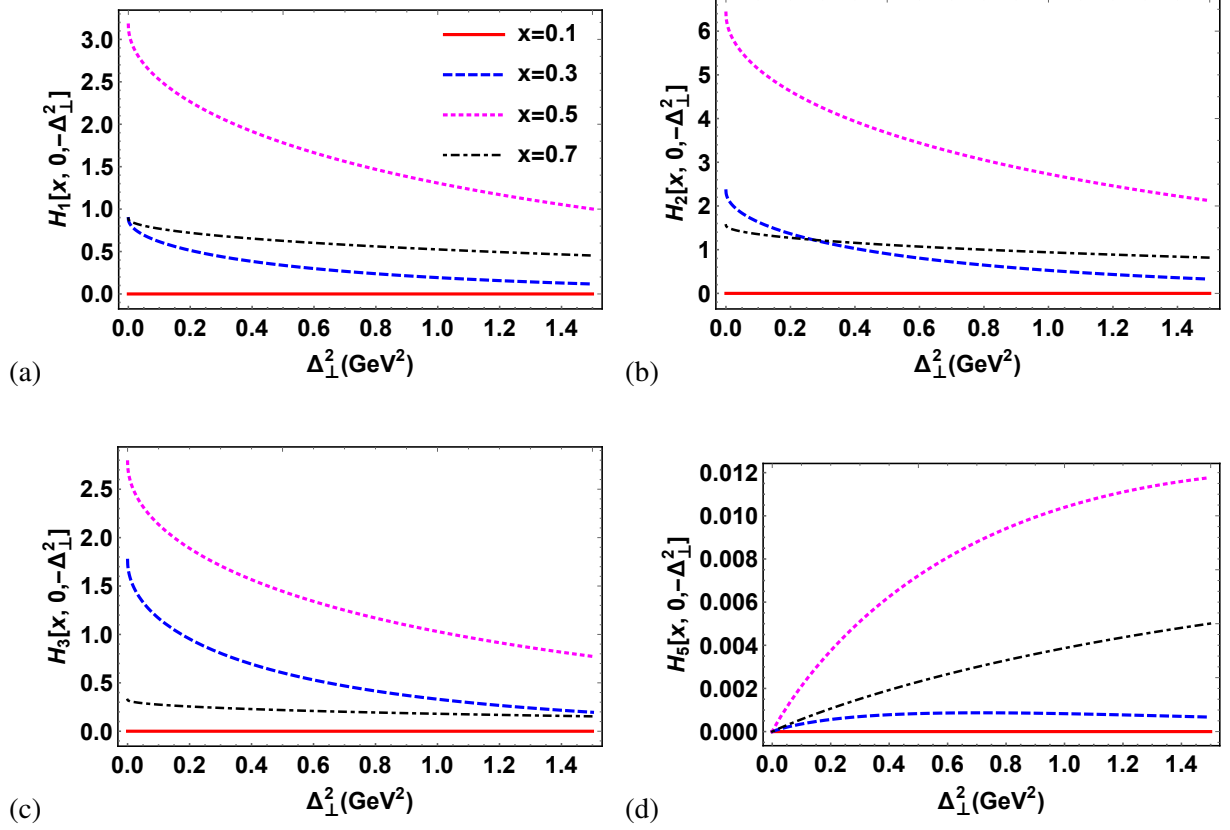


FIG. 6: (Color online) The quark GPDs of  $J/\psi$ -meson (a)  $H_1(x, 0, -\Delta_{\perp}^2)$ , (b)  $H_2(x, 0, -\Delta_{\perp}^2)$ , (c)  $H_3(x, 0, -\Delta_{\perp}^2)$ , and (d)  $H_5(x, 0, -\Delta_{\perp}^2)$  have been plotted with respect to  $\Delta_{\perp}^2$  at fixed value of longitudinal momentum fraction  $x = 0.1, 0.3, 0.5$  and  $0.7$ .

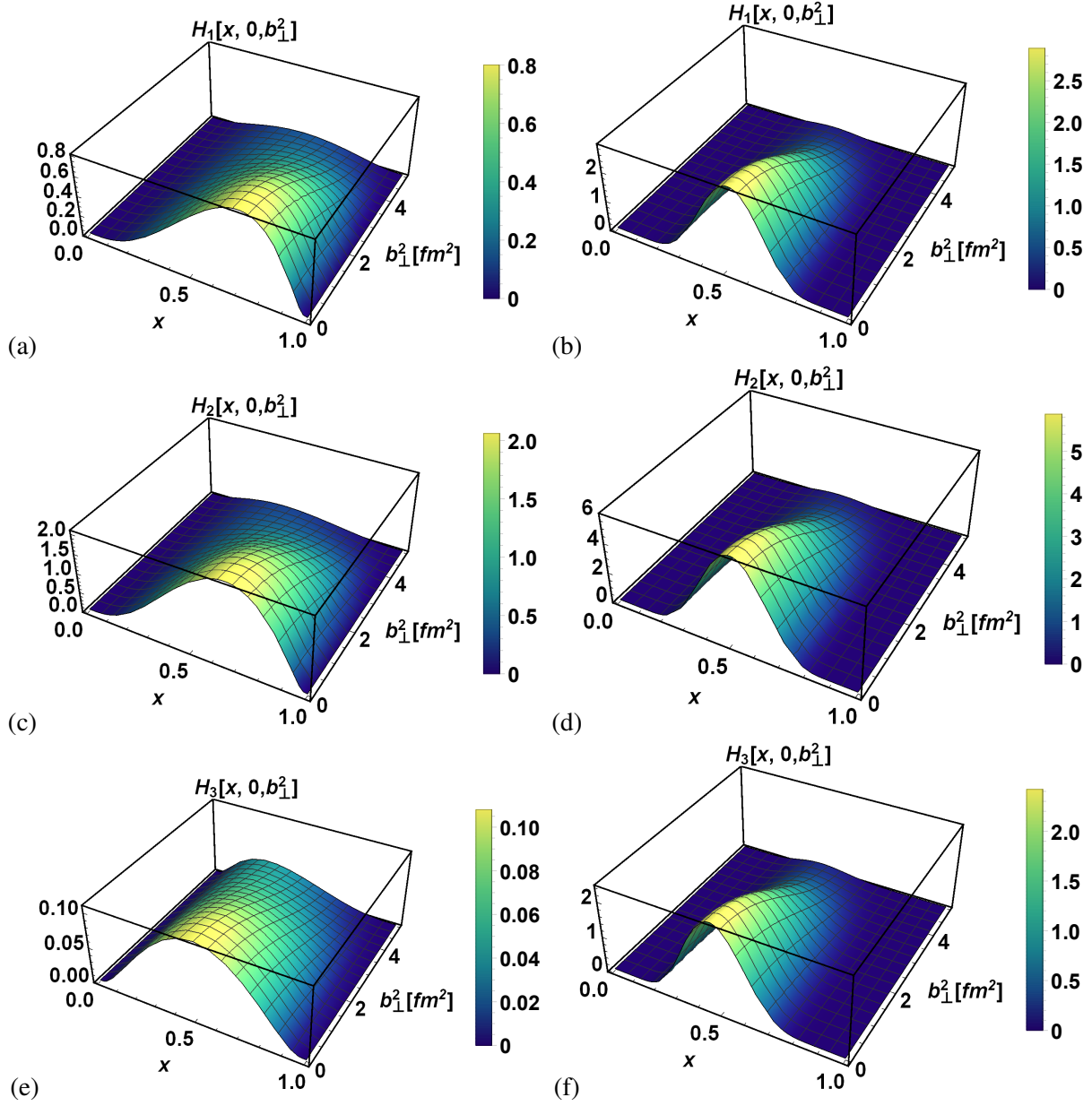


FIG. 7: (Color online) The  $H_1(x, 0, b_{\perp}^2)$ ,  $H_2(x, 0, b_{\perp}^2)$ , and  $H_3(x, 0, b_{\perp}^2)$  quark GPDs for  $\rho$ -meson (left panel (a), (c), and (e)) and  $J/\psi$ -meson (right panel (b), (d), and (f)) have been plotted with respect to  $b_{\perp}^2$  ( $\text{fm}^2$ ) and longitudinal momentum fraction  $x$ .

### III. UNPOLARIZED QUARK GPDS

The amplitudes in DVCS and deep exclusive meson electroproduction (DEMP) on a spin-one target are determined by non-perturbative matrix components that are parametrized in terms of nine GPDs for the quark sector out of which five are unpolarized GPDs. The correlation function for the unpolarized quark GPDs of spin-1 mesons is expressed through the quark-quark correlator as [44, 47, 49]

$$V_{S'_z, S_z}(x, \xi, -\Delta_\perp^2) = \int \frac{dz^-}{2\pi} e^{ixP_a^+ z^-} \langle M(P'^+, \mathbf{P}'_\perp, S'_z) | \bar{\psi}\left(-\frac{z^-}{2}\right) \gamma^+ \psi\left(\frac{z^-}{2}\right) | M(P^+, \mathbf{P}_\perp, S_z) \rangle. \quad (20)$$

Here,  $V_{S'_z, S_z}(x, \xi, -\Delta_\perp^2)$  is the light-front (LF) overlap correlation function between the initial and final state meson.  $P$  and  $P'$  are the four-momenta of the initial and final state of the meson having spin projections  $S_z$  and  $S'_z$ , respectively.  $P_a = (P' + P)/2$  is the average momentum of the meson.  $\Delta(\Delta^+, \Delta^-, \Delta_\perp) = P' - P$  is the momentum transferred between the final and initial meson states. The skewness variable is denoted by  $\xi = \frac{-\Delta^+}{2P_a^+}$ . However, for this work, we have not considered the longitudinal momentum transfer between the initial and final state mesons, therefore,  $\xi = 0$  as  $\Delta^+ = 0$ . Consequently, the correlator can be decomposed to five spin-1 unpolarized GPDs having the form  $V_{S'_z, S_z}(x, \xi = 0, -\Delta_\perp^2)$  as [48, 49]

$$\begin{aligned} V_{S'_z, S_z}(x, 0, -\Delta_\perp^2) = & -(\epsilon'^* \cdot \epsilon) H_1(x, 0, -\Delta_\perp^2) + \frac{(\epsilon \cdot n)(\epsilon' \cdot P) + (\epsilon' \cdot n)(\epsilon \cdot P)}{P \cdot n} H_2(x, 0, -\Delta_\perp^2) \\ & - 2 \frac{(\epsilon \cdot P)(\epsilon'^* \cdot P)}{M_{q\bar{q}}^2} H_3(x, 0, -\Delta_\perp^2) + \frac{(\epsilon \cdot n)(\epsilon' \cdot P) - (\epsilon'^* \cdot n)(\epsilon \cdot P)}{P \cdot n} H_4(x, 0, -\Delta_\perp^2) \\ & + \left\{ M_{q\bar{q}}^2 \frac{(\epsilon \cdot n)(\epsilon' \cdot n)}{(P \cdot n)^2} + \frac{1}{3}(\epsilon'^* \cdot \epsilon) \right\} H_5(x, 0, -\Delta_\perp^2), \end{aligned} \quad (21)$$

with  $\epsilon \equiv \epsilon(P, S_z)$  and  $\epsilon' \equiv \epsilon(P', S'_z)$  being the polarization vector of the initial and final state meson (discussed in Eq. (15)). The four-vector notations used in the above equation are expressed in the Breit frame as [49, 64]

$$n = (0, \sqrt{2}, 0, 0), \quad (22)$$

$$\Delta = (0, 0, \Delta_\perp, 0), \quad (23)$$

$$P = \frac{M_{q\bar{q}}}{\sqrt{2}} (\sqrt{1+\eta}, \sqrt{1+\eta}, -\frac{\Delta_\perp}{M_{q\bar{q}}\sqrt{2}}, 0), \quad (24)$$

$$P' = \frac{M_{q\bar{q}}}{\sqrt{2}} (\sqrt{1+\eta}, \sqrt{1+\eta}, \frac{\Delta_\perp}{M_{q\bar{q}}\sqrt{2}}, 0). \quad (25)$$

Here,  $\eta = \frac{\Delta_\perp^2}{4M_{q\bar{q}}^2}$ . Consequently, the LF overlap correlation function  $V_{S'_z, S_z}(x, \xi, -\Delta_\perp^2)$  obey the parity and time reversal invariance as [44, 49, 71]

$$V_{S'_z, S_z}(x, 0, -\Delta_\perp^2) = (-1)^{S'_z - S_z} V_{-S'_z, -S_z}(x, 0, -\Delta_\perp^2), \quad (26)$$

$$V_{S'_z, S_z}(x, \xi, -\Delta_\perp^2) = (-1)^{S'_z - S_z} V_{S'_z, S_z}(x, -\xi, -\Delta_\perp^2). \quad (27)$$

Now, applying the above parity and time-reversal condition to calculate the unpolarized quark GPDs at zero skewness, we are left with four independent  $V_{S'_z, S_z}(x, \xi, -\Delta_\perp^2)$  functions in the form of different spin projections, which are  $V_{0,0}(x, 0, -\Delta_\perp^2)$ ,  $V_{0,1}(x, 0, -\Delta_\perp^2)$ ,  $V_{1,1}(x, 0, -\Delta_\perp^2)$ , and  $V_{1,-1}(x, 0, -\Delta_\perp^2)$ . Reversing Eq. (22), by using the meson momentum and polarization vector, the unpolarized GPDs are found to be

$$H_1(x, 0, -\Delta_\perp^2) = \frac{1}{3} [V_{0,0}(x, 0, -\Delta_\perp^2) - 2(\eta - 1)V_{1,1}(x, 0, -\Delta_\perp^2) + 2\sqrt{2\eta}V_{1,0}(x, 0, -\Delta_\perp^2) + 2V_{1,-1}(x, 0, -\Delta_\perp^2)], \quad (28)$$

$$H_2(x, 0, -\Delta_\perp^2) = 2V_{1,1}(x, 0, -\Delta_\perp^2) - \frac{2}{\sqrt{2\eta}}V_{1,0}(x, 0, -\Delta_\perp^2), \quad (29)$$

$$H_3(x, 0, -\Delta_\perp^2) = -\frac{V_{1,-1}(x, 0, -\Delta_\perp^2)}{\eta}, \quad (30)$$

$$H_4(x, 0, -\Delta_\perp^2) = 0, \quad (31)$$

$$H_5(x, 0, -\Delta_\perp^2) = V_{0,0}(x, 0, -\Delta_\perp^2) - (1 + 2\eta)V_{1,1} + 2\sqrt{2\eta}V_{1,0}(x, 0, -\Delta_\perp^2) - V_{1,-1}(x, 0, -\Delta_\perp^2). \quad (32)$$

The LF overlap correlation function  $V_{S'_z, S_z}(x, 0, -\Delta_\perp^2)$  can be written in the overlap form of LFWFs of the total meson wave function as

$$V_{S'_z, S_z}(x, 0, -\Delta_\perp^2) = \sum_{\lambda_1, \lambda_2} \int \frac{d^2\mathbf{k}_\perp}{2(2\pi)^3} \Psi_{S'_z}^*(x, \mathbf{k}'_\perp, \lambda_1, \lambda_2) \Psi_{S_z}(x, \mathbf{k}_\perp, \lambda_1, \lambda_2). \quad (33)$$

Here,  $\mathbf{k}'_\perp = \mathbf{k}_\perp + (1-x)\Delta_\perp$  and  $\mathbf{k}_\perp$  are the transverse momentum of the quark of the final and initial meson.  $H_4$  quark GPD for our case is found to be zero similar to NJL model, DS-BSE approach, BLFQ, and LFQM.

The behavior of these unpolarized quark GPDs for  $\rho$ -meson have been provided through three-dimensional plots in Fig. 1 as a function of longitudinal momentum fraction  $x$  and squared momentum transferred  $\Delta_\perp^2$ .  $H_1(x, 0, -\Delta_\perp^2)$  quark GPD shows a smooth, positive distributions all over, and symmetric behavior at around  $x = 0.5$  at  $\Delta_\perp = 0$  under  $x \leftrightarrow (1-x)$  as shown in Fig. 1 (a), reflecting the equal constituent quark masses of  $\rho$ -meson. A similar kind of positive distributions of  $H_1(x, 0, -\Delta_\perp^2)$  can also be seen in LFQM [47] and NJL model [45]. The symmetric behavior



at  $\Delta_\perp^2 = 0$  observed is in line with the NJL model with the distribution nearly vanishing around the end points  $x = 0$  and  $x = 1$ . As  $\Delta_\perp^2$  increases, the distribution  $H_1(x, 0, -\Delta_\perp^2)$  peak suppresses and becomes zero after  $\Delta_\perp \geq 1.2$  GeV. A higher peak is observed in the  $H_2(x, 0, -\Delta_\perp^2)$  quark GPD as compared to other quark GPDs as shown in Fig. 1. It has more of a sharp symmetric behavior around  $x \approx 0.6 - 0.7$  with larger amplitude. The  $H_2(x, 0, -\Delta_\perp^2)$  exhibits stronger suppression and a noticeable shift of the peak toward higher  $x$  as  $\Delta_\perp^2$  increases. The GPDs  $H_2(x, 0, -\Delta_\perp^2)$  and  $H_3(x, 0, -\Delta_\perp^2)$  show positive distributions in the entire range of  $x$  and  $\Delta_\perp$  similar to NJL model observations [45]. In case of LFQM,  $H_2$  shows positive distribution whereas  $H_3$  has both positive and negative distribution clearly contradicting our model results.

The  $H_5(x, 0, -\Delta_\perp^2)$  quark GPD has a lower peak amplitude distribution compared to others and have zero distribution at  $\Delta_\perp = 0$ . The terms  $V_{0,0}$  and  $V_{1,1}$  show the contribution of S-wave as there is no increment in orbital angular momentum ( $L_z = 0$ ), whereas the contribution of the P-wave is shown by the presence of  $V_{1,0}$  term indicating the increment in the angular momentum by unity ( $L_z = \pm 1$ ). Additionally, the term  $V_{1,-1}$  contributes to the presence of D-wave as the orbital angular momentum is raised by two units ( $L_z = \pm 2$ ). Consequently, the quark GPDs  $H_{1(5)}(x, 0, -\Delta_\perp^2)$  include the superposition of S, P, and D-wave, whereas only  $H_2(x, 0, -\Delta_\perp^2)$  contributes S and P-wave, and  $H_5(x, 0, -\Delta_\perp^2)$  only contains D-wave. In Figs. 2 and 3, we have plotted the quark GPDs of  $\rho$ -meson with respect to  $x$  at fixed values of  $\Delta_\perp$  and with respect to  $\Delta_\perp$  at fixed values of  $x$ , respectively. We observed that the distribution decreases with  $x$  with an increase in momentum transferred between the states for all the quark GPDs except  $H_5$ . For the case  $H_5$ , we found that the distribution shows both negative and positive behavior, and with an increase in  $\Delta_\perp$ , the positive distribution increases. This kind of behavior shows up to  $\Delta_\perp^2 = 20 \text{ GeV}^2$ , after which the distribution becomes zero. A similar kind of behavior is also seen with an increase in  $x$  also.

To have an idea about the heavy quark structure, we have also studied the quark GPDs of the heavy charmonia  $J/\psi$  vector meson. The quark GPDs of  $J/\psi$ -meson have been plotted with respect to  $x$  and  $\Delta_\perp^2$  through three-dimensional and two-dimensional plots in Figs. 4-6. All the quark GPDs are found to have maximum distributions around  $x = 0.5$  and show  $x \leftrightarrow (1 - x)$  symmetry. The distributions of quark GPDs decrease with an increase in  $\Delta_\perp$ , as like the  $\rho$ -meson case. The  $H_5$  quark GPD shows only positive behavior for the case of  $J/\psi$ -meson. We observed that  $H_{1,2,3}$  quark GPDs of our results have a similar kind of trend with BLFQ results [48]. Overall, we found that the momentum fraction carried by the quark decreases with an increase in momentum transferred to the final state meson.

All these quark GPDs have also been plotted in impact parameter space by taking the Fourier transform of  $\Delta_\perp$  as

$$H_i(x, 0, b_\perp^2) = \int \frac{d^2\Delta_\perp}{(2\pi)^2} e^{-ib_\perp \cdot \Delta_\perp} H_i(x, 0, -\Delta_\perp^2). \quad (34)$$

These quark GPDs at impact parameter space have been studied using the three-dimensional plots in Fig. 7 for both light  $\rho$  and heavy  $J/\psi$  vector mesons. All the quark GPDs are found to have positive distributions with a sharply decreasing behavior with maximum distributions at  $b_\perp = 0$ .

### A. Vector meson Form Factors

There are a total of three electromagnetic form factors ( $F_i(Q^2)(i = 1, 2, 3)$ ) present at the leading twist for the spin-1 vector mesons case. These form factors can be calculated either by solving the quark-quark correlation function or from unpolarized quark GPDs. These Lorentz invariant form factors are defined by the matrix elements of the  $J^\mu$  current sandwiched between initial  $|M(P^+, \mathbf{P}_\perp, S_z\rangle$  and final  $\langle M(P'^+, \mathbf{P}'_\perp, S'_z|$  states as follows [47, 52]

$$\begin{aligned} \langle M(P'^+, S'_z | J^\mu | M(P^+, \mathbf{P}_\perp, S_z) \rangle = & -\epsilon' \cdot \epsilon (P + P')^\mu F_1(Q^2) + (\epsilon' n \cdot \epsilon' - \epsilon' n \cdot \epsilon) F_2(Q^2) + \\ & \frac{(\epsilon' \cdot n)(\epsilon \cdot n)}{2M_v^2} (P + P')^\mu F_3(Q^2), \end{aligned} \quad (35)$$

where  $Q^2 = \Delta^2 = -\Delta_\perp^2$ . On the other hand, these form factors can be calculated from the unpolarized quark GPDs as

$$\int_{-1}^1 dx H_i(x, 0, -\Delta_\perp^2) = F_i(Q^2), \quad (i = 1, 2, 3) \quad (36)$$

$$\int_{-1}^1 dx H_i(x, \xi, -\Delta_\perp^2) = 0. \quad (i = 4, 5) \quad (37)$$

Both calculations give rise to equal form factor results. These form factors have been plotted with respect to  $Q^2$  GeV<sup>2</sup> in Fig. 8 for both  $\rho$  and  $J/\psi$  vector mesons. All the form factors are found to have positive distributions and have a maximum distribution at  $Q^2 = 0$ . It is observed that  $F_2(Q^2)$  has higher distributions compared to other form factors for both the particles. These form factors can be used to calculate the charge, magnetic, and quadrupole form factors of vector mesons. These can be calculated as

$$G_C(Q^2) = (1 + \frac{2}{3}\eta)F_1(Q^2) + \frac{2}{3}\eta F_2(Q^2) + \frac{2}{3}\eta(1 + \eta)F_3(Q^2), \quad (38)$$

$$G_M(Q^2) = F_2(Q^2), \quad (39)$$

$$G_Q(Q^2) = F_1(Q^2) + F_2(Q^2) + (1 + \eta)F_3(Q^2). \quad (40)$$

The light  $\rho$ -meson and heavy  $J/\psi$ -meson form factors have been plotted in Figs. 9 and 10 with respect to  $Q^2$  GeV<sup>2</sup>, respectively. All the form factors of  $\rho$ -meson have been compared with lattice simulation results [72] up to  $Q^2 = 3$  GeV<sup>2</sup> and are found to have a similar trend but lower distributions except for the case of  $G_Q$ . At  $Q^2 = 0$ ,  $G_C$ ,  $G_M$ , and  $G_Q$  are found to be unity, 2.1, and zero for both the particles, respectively. For a better understanding of these form factors, we have compared our results with theoretical model results [50, 54–58] up to  $Q^2 = 10$  GeV<sup>2</sup> in Figs. 9 (e) and (f). The charge  $G_C$  and magnetic  $G_M$  form factors are found to have a similar trend but with lower distributions compared to the NJL model [45, 73], LFCQM [47], DS-BSE [49], contact interaction [74], AdS/QCD model [59], LFCQM [50], BLFQ [48] and other models [54–58] results. However, the quadrupole form factor  $G_Q$ , on the one hand, has a opposite kind of behavior at low  $Q^2$  compared to Refs. [45, 47, 49, 58, 73, 74], whereas, on the other hand, it has the same kind of trend with Refs. [48, 55–57] as shown in Fig. 9 (f). The charge form factor  $G_C$  shows negative distribution after  $Q^2 \geq 4$  GeV<sup>2</sup> as like NJL model [45], LFCQM [50] and other models [54–57] as shown in Fig. 9 (e). We have also observed that the heavier  $J/\psi$ -meson has higher form factor distributions compared to the light  $\rho$ -meson as shown in Fig. 10. We have also observed that the asymptotic limit of QCD reported in Refs. [56, 74] is strictly followed by our model, which reads as

$$G_C(Q^2) : G_M(Q^2) : G_Q(Q^2) \xrightarrow{Q^2 \rightarrow \infty} 1 - \frac{2\eta}{3} : 2 : -1. \quad (41)$$

At zero momentum transfer  $Q^2 = 0$ , one can find the charge, magnetic moment ( $\mu_p$ ), and quadrupole moment  $Q_p$  of the vector mesons from these form factors as

$$eG_C(Q^2 = 0) = e, \quad G_M(Q^2 = 0) = \mu_p, \quad G_Q(Q^2 = 0) = Q_p. \quad (42)$$

Here,  $e$  is the static charge.  $\mu_p$  and  $Q_p$  are in the units of Bohr magneton  $e/2M_{\rho(J/\psi)}$  and  $e/M_{\rho(J/\psi)}^2$  respectively. Here,  $M_{\rho(J/\psi)}$  is the physical mass of  $\rho$  and  $J/\psi$ -mesons. The charge radii  $\sqrt{\langle r_c^2 \rangle}$  of the respective vector mesons can be calculated using the fundamental radius equation as

$$\langle r_c^2 \rangle = \frac{-6}{G_C(0)} \frac{\partial G_C(Q^2)}{\partial Q^2} \Big|_{Q^2 \rightarrow 0}. \quad (43)$$

$G_C(0)$  in this case is unity. The value of charge radii  $\sqrt{\langle r_c^2 \rangle}$ , magnetic moment  $\mu_p$ , and quadrupole moment  $Q_p$  have been presented in Table I for both particles along with the comparison with available predictions [61, 74–78]. We observe that our charge radii values are slightly higher than other results whereas  $\mu_p$  and  $Q_p$  are in good agreement with them.

Futher, using  $G_C(Q^2)$ ,  $G_M(Q^2)$ , and  $G_Q(Q^2)$  form factors, one can define the conserving ( $G_{++}^+(Q^2)$  and  $G_{00}^+(Q^2)$ ) and non-conserving ( $G_{-+}^+(Q^2)$  and  $G_{0+}^+(Q^2)$ ) helicity matrix element as

$$G_{++}^+(Q^2) = \frac{1}{1+\eta} \left( G_C(Q^2) + \eta G_M(Q^2) + \frac{\eta}{3} G_Q(Q^2) \right), \quad (44)$$

$$G_{00}^+(Q^2) = \frac{1}{1+\eta} \left( (1-\eta) G_C(Q^2) + 2\eta G_M(Q^2) - \frac{2\eta}{3} (1+2\eta) G_Q(Q^2) \right), \quad (45)$$

$$G_{0+}^+(Q^2) = -\frac{\sqrt{2\eta}}{1+\eta} \left( G_C(Q^2) - \frac{1}{2} (1-\eta) G_M(Q^2) + \frac{\eta}{3} G_Q(Q^2) \right), \quad (46)$$

$$G_{-+}^+(Q^2) = \frac{\eta}{1+\eta} \left( G_C(Q^2) - G_M(Q^2) - (1 + \frac{2\eta}{3}) G_Q(Q^2) \right). \quad (47)$$

Here,  $+$ ( $-$ ) denote the  $+1$ ( $-1$ ) spin projections. These matrix elements have been plotted in Fig. 11 for both the mesons. Both the conserving matrix elements  $G_{++}^+$  and  $G_{00}^+$  shows positive behavior and are found to be unity at  $Q^2 = 0$ . A similar kind of results have also been seen in NJL model [73] and LFQM [47]. The non-conserving ( $G_{-+}^+(Q^2)$  and  $G_{0+}^+(Q^2)$ ) helicity matrix elements show both positive and negative distributions. The  $G_{0+}^+$  elements have negative distribution in between  $0.1 \leq Q^2 \leq 2.1 \text{ GeV}^2$ , while  $G_{-+}^+$  shows negative distributions around  $0 \leq Q^2 \leq 1.7 \text{ GeV}^2$ . In the case of LFQM [47] and NJL model [73], the non-conserving  $G_{-+}^+$  matrix element shows only a negative distribution. Another important observation in this regard is that the non-conserving matrix elements have lower distributions compared to the conserving matrix elements.

An important reason to study these  $G_C(Q^2)$ ,  $G_M(Q^2)$ , and  $G_Q(Q^2)$  form factors is that they can be directly connected with the Rosenbluth cross section [53] for elastic electron scattering on a target of arbitrary spin in the laboratory frame through  $A(Q^2)$  and  $B(Q^2)$  structure function along with tensor polarization  $T_{20}(Q^2, \phi)$ . The  $A(Q^2)$ ,  $B(Q^2)$ , and  $T_{20}(Q^2, \phi)$  can be calculated from  $G_C(Q^2)$ ,  $G_M(Q^2)$ , and  $G_Q(Q^2)$  as [73, 79]

$$A(Q^2) = G_C^2(Q^2) + 2/3 \eta G_M^2(Q^2) + 2(2/3)^2 \eta^2 G_Q^2(Q^2), \quad (48)$$

$$B(Q^2) = \frac{4}{3} \eta (1 + \eta) G_M^2, \quad (49)$$

$$T_{20}(Q^2, \phi) = -\eta \frac{\sqrt{2} \frac{4}{3} \eta G_Q^2(Q^2) + 4 G_Q(Q^2) G_C(Q^2) + (1/2 + (1 + \eta \tan^2 \frac{\phi}{2})) G_M^2(Q^2)}{A(Q^2) + B(Q^2) \tan^2 \frac{\phi}{2}}. \quad (50)$$

Using these, the cross-section of can be calculated as [53, 73]

$$\frac{d\sigma}{d(-Q^2)} = \frac{4\pi\alpha^2}{(-Q^2)^2} \left[ \left( 1 + \frac{(-Q^2)s}{(s - M_{\rho(J/\psi)}^2)^2} \right) A(Q^2) - \frac{M_{\rho(J/\psi)}^2 (-Q^2)}{(s - M_{\rho(J/\psi)}^2)^2} B(Q^2) \right]. \quad (51)$$

As there is no experimental data available for  $A(Q^2)$  and  $B(Q^2)$  structure functions, our results can be compared with the NJL model calculations [73] which exhibits a similar behavior as shown in

Fig. 12. The  $A(Q^2)$  structure function saturates after  $Q^2 = 1.5 \text{ GeV}^2$ , as in the case of NJL model and LFQM [52]. Analogous to the form factor results, the structure functions also have a similar kind of distribution with slighter magnitudes. For the case of heavy  $J/\psi$ -vector meson, the  $B(Q^2)$  structure function is very low compared to the  $\rho$ -meson. However, both the structure and function obey the sum rule

$$A(Q^2 = 0) = 1, \quad B(Q^2 = 0) = 0. \quad (52)$$

#### IV. SPIN-1 PARTON DISTRIBUTION FUNCTIONS

Without knowing the parton's inherent transverse momentum, the PDFs encode the longitudinal momentum distribution and the polarization carried by the partons at  $P = P'$  and  $\Delta_\perp = 0$ . For the case of spin-1 vector mesons, there are a total of four quark PDFs present at the leading twist, which are unpolarized  $f_1(x)$ , transversity polarized  $h_1(x)$ , helicity  $g_1(x)$ , and tensor polarized  $f_{1LL}(x)$  quark PDFs [80]. From the unpolarized GPDs, we can only derive quark  $f_1(x)$  and  $f_{1LL}(x)$  PDFs. For the polarized quark  $g_1(x)$  and  $h_1(x)$  PDFs, we have considered the possible LFWFs. These quark PDFs can be calculated using the overlap form of LFWFs and from GPDs limit as [31, 45, 62, 81]

$$\begin{aligned} f_1(x) &= H_1(x, 0, 0), \\ &= \int \frac{d^2 \mathbf{k}_\perp}{2(2\pi)^3} \frac{1}{3} \sum_{\lambda_1, \lambda_2} \left( |\Psi_{S_z=0}(x, \mathbf{k}_\perp, \lambda_1, \lambda_2)|^2 + |\Psi_{S_z=1}(x, \mathbf{k}_\perp, \lambda_1, \lambda_2)|^2 + |\Psi_{S_z=-1}(x, \mathbf{k}_\perp, \lambda_1, \lambda_2)|^2 \right), \end{aligned} \quad (53)$$

$$\begin{aligned} f_{1LL}(x) &= H_5(x, 0, 0) \\ &= b_1(x) \\ &= \int \frac{d^2 \mathbf{k}_\perp}{2(2\pi)^3} \sum_{\lambda_1, \lambda_2} \left( |\Psi_{S_z=0}(x, \mathbf{k}_\perp, \lambda_1, \lambda_2)|^2 - (|\Psi_{S_z=1}(x, \mathbf{k}_\perp, \lambda_1, \lambda_2)|^2 + |\Psi_{S_z=-1}(x, \mathbf{k}_\perp, \lambda_1, \lambda_2)|^2) \right), \end{aligned} \quad (54)$$

$$\begin{aligned} h_1(x) &= \int \frac{d^2 \mathbf{k}_\perp}{2(2\pi)^3} \frac{1}{2\sqrt{2}} \sum_{\lambda_1, \lambda_2} \left( \Psi_{S_z=1}^*(x, \mathbf{k}_\perp, \uparrow, \lambda_2) \Psi_{S_z=0}(x, \mathbf{k}_\perp, \downarrow, \lambda_2) + \Psi_{S_z=0}^*(x, \mathbf{k}_\perp, \downarrow, \lambda_2) \Psi_{S_z=1}(x, \mathbf{k}_\perp, \uparrow, \lambda_2) \right. \\ &\quad \left. + \Psi_{S_z=-1}^*(x, \mathbf{k}_\perp, \downarrow, \lambda_2) \Psi_{S_z=0}(x, \mathbf{k}_\perp, \uparrow, \lambda_2) + \Psi_{S_z=0}^*(x, \mathbf{k}_\perp, \uparrow, \lambda_2) \Psi_{S_z=-1}(x, \mathbf{k}_\perp, \downarrow, \lambda_2) \right), \end{aligned} \quad (55)$$

$$\begin{aligned} g_1(x) &= \int \frac{d^2 \mathbf{k}_\perp}{2(2\pi)^3} \frac{1}{2} \sum_{\lambda_1, \lambda_2} \left( |\Psi_{S_z=1}(x, \mathbf{k}_\perp, \uparrow, \lambda_2)|^2 - |\Psi_{S_z=1}(x, \mathbf{k}_\perp, \downarrow, \lambda_2)|^2 \right. \\ &\quad \left. + |\Psi_{S_z=-1}(x, \mathbf{k}_\perp, \downarrow, \lambda_2)|^2 - |\Psi_{S_z=-1}(x, \mathbf{k}_\perp, \uparrow, \lambda_2)|^2 \right). \end{aligned} \quad (56)$$

The explicit form of these quark PDFs have been given in the appendix (Sec. VII). The tensor polarized  $f_{1LL}$  carries information about the  $b_1$  structure function of the vector mesons [82]. However, in this work, the  $f_{1LL}(x)$  is found to be zero. Further, these PDFs obey the sum rule

$$\int f_1(x)dx = 1, \quad \int f_{1LL}(x)dx = b_1(x)dx = 0. \quad (57)$$

These quark PDFs have been plotted with respect to the longitudinal momentum fraction  $x$  in Figs. 13 and 14 for both light  $\rho$  and heavy  $J/\psi$  vector mesons, respectively. The PDFs have been plotted at the model scale ( $\mu^2 = 0.19 \text{ GeV}^2$ ) as well as at  $\mu^2 = 5 \text{ GeV}^2$  for which the evolution has been carried out using next to next to leading order Dokshitzer–Gribov–Lipatov–Altarelli–Parisi (DGLAP) equations [83–85]. All the quark PDFs are found to have positive distributions and a maxima after  $x = 0.5$ . From the  $\rho$ -meson quark PDFs, we observe that unpolarized  $f_1(x)$  have higher distributions compared to  $g_1(x)$  and  $h_1(x)$  quark PDFs. Similar trend can also be seen at  $\mu^2 = 5 \text{ GeV}^2$ . The  $\rho$ -meson quark PDFs have been explored in NJL model [86, 87], DS-BSE approach [49], LFHM [69] etc. Our results are found to have a similar kind of positive distributions as in these models. The tensor  $f_{1LL}$  quark PDF is found to be zero for both the particles. Due to heavy quark mass of the  $J/\psi$ -meson, the quark PDFs show a sharp distribution around  $x = 0.5$  and a symmetry  $x \leftrightarrow (1 - x)$ . We observe that there is no distribution of quark PDFs below  $x \leq 0.2$  and above  $x \geq 0.8$  for  $J/\psi$ -meson. In LFHM [31], DS-BSE approach [49], BLFQ [88], and in Ref. [89], similar results and behavior have been reported. The positivity constraints on the PDFs mentioned in Refs. [31, 69, 86] of spin-1 mesons are also verified in our calculations. The average momentum fraction of order  $n$  (Mellin moments) carried by the quark PDFs can be calculated as

$$\langle x^n \rangle = \frac{\int dx x^n PDFs}{\int dx PDFs}. \quad (58)$$

The  $\langle x^n \rangle$  of both particles has been presented in Table II. It is clear from the results that the unpolarized  $f_1(x)$  carry the highest average momenta as compared to the other PDFs.

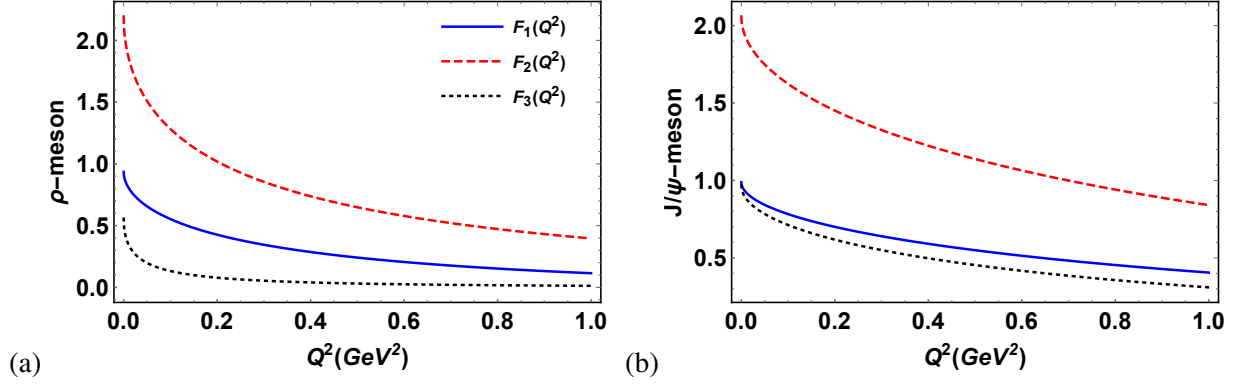


FIG. 8: (Color online) The elastic form factors  $F_1(Q^2)$ ,  $F_2(Q^2)$ , and  $F_3(Q^2)$  have been plotted with respect to  $Q^2$  for (a) light  $\rho$  and (b) heavy  $J/\psi$  vector meson.

		$\sqrt{\langle r_c^2 \rangle}$ fm	$\mu_p$	$Q_p$
$\rho(u\bar{d})$	Our result	0.95	2.19	-0.023
	Ref. [75]	0.73	2.01	-0.026
	Ref. [78]	0.82	2.07	-0.045
	Ref. [61]	0.82	2.48	-0.070
	Ref. [74]	0.56	0.75	-
	Ref. [77]	1.12	2.54	-
$J/\psi(c\bar{c})$	Our result	0.69	2.05	-0.006
	Ref. [74]	0.350	2.03	-
	Ref. [75]	0.24	2.12	-
	Ref. [76]	0.066	2.10	-

TABLE I: The charge radii  $\sqrt{\langle r_c^2 \rangle}$  (in fm), magnetic moment  $\mu_p$  (in units of Bohr magneton), and quadrupole moment  $Q_p$  (in fm<sup>2</sup>) of light  $\rho$  and heavy  $J/\psi$  vector mesons have been compared with available data [61, 74–78].

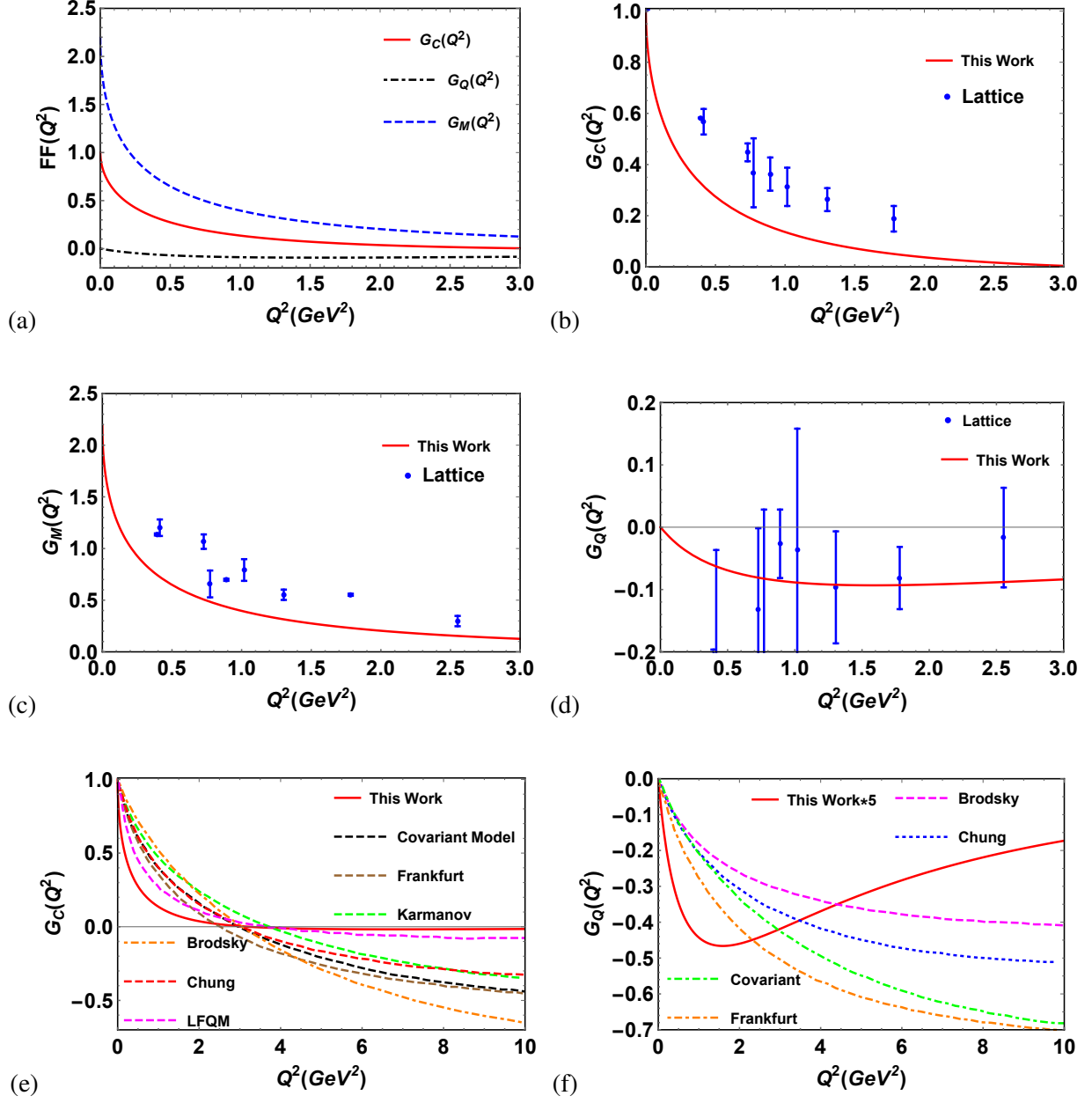


FIG. 9: (Color online) (a) The charge ( $G_C(Q^2)$ ), magnetic ( $G_M(Q^2)$ ), and quadrupole ( $G_Q(Q^2)$ ) form factors have been plotted with respect to  $Q^2$  for  $\rho$ -meson. The charge ( $G_C(Q^2)$ ), magnetic ( $G_M(Q^2)$ ), and quadrupole ( $G_Q(Q^2)$ ) form factors have been compared with available lattice simulations data [72] in (b), (c), and (d), respectively. The charge  $G_C(Q^2)$  and quadrupole  $G_Q(Q^2)$  form factors have been compared with available theoretical models [50, 54–58].



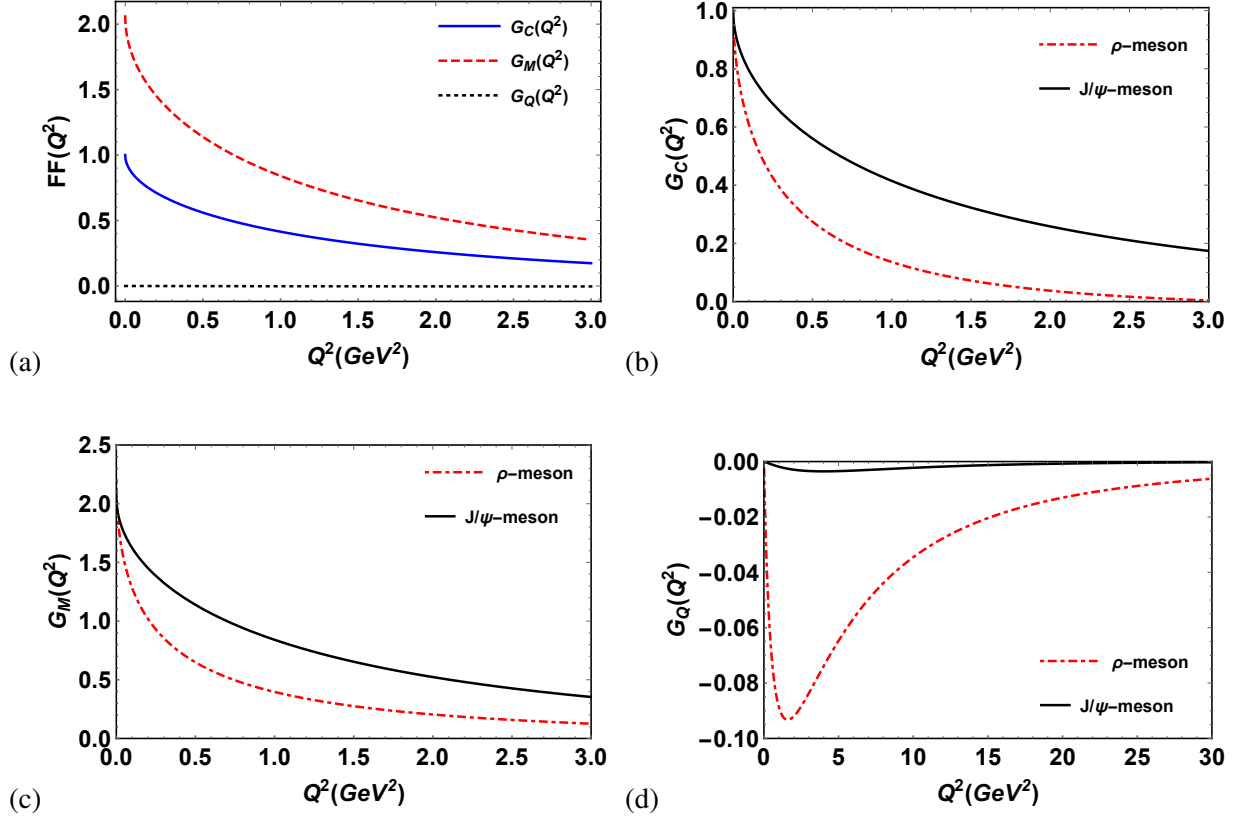


FIG. 10: (Color online) (a) The charge ( $G_C(Q^2)$ ), magnetic ( $G_M(Q^2)$ ), and quadrupole ( $G_Q(Q^2)$ ) form factors have been plotted with respect to  $Q^2$  for  $J/\psi$ -meson. The charge ( $G_C(Q^2)$ ), magnetic ( $G_M(Q^2)$ ), and quadrupole ( $G_Q(Q^2)$ ) form factors of  $J/\psi$ -meson have been compared with  $\rho$ -meson form factors in (b), (c), and (d), respectively.

PDFs	$\langle x^0 \rangle$		$\langle x^1 \rangle$	
	$\rho$	$J/\psi$	$\rho$	$J/\psi$
$f_1(x)$	1	1	0.5	0.5
$g_1(x)$	0.559	0.932	0.314	0.467
$h_1(x)$	0.779	0.966	0.392	0.483

TABLE II: The average longitudinal momentum fractions  $\langle x^{0(1)} \rangle$  for both  $\rho$  and  $J/\psi$  vector mesons.

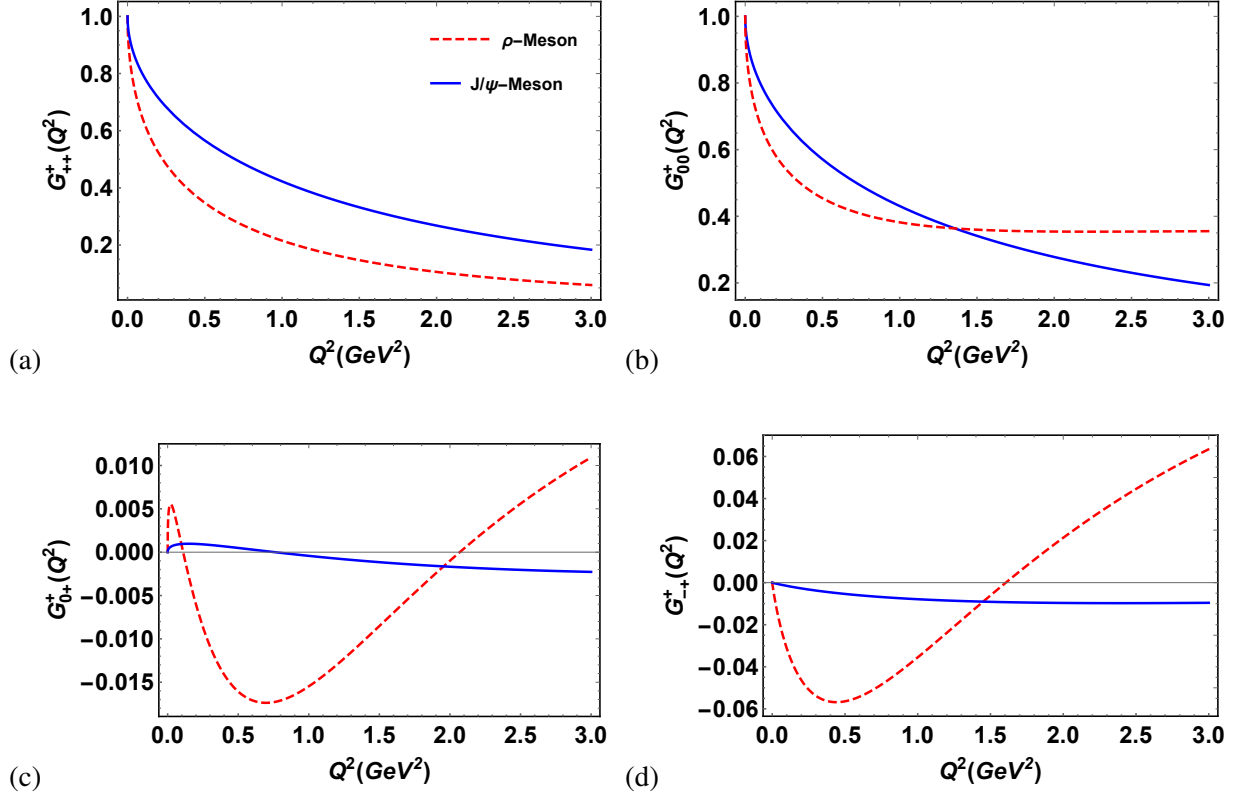


FIG. 11: (Color online) The helicity-conserving matrix elements  $G_{++}^+(Q^2)$  and  $G_{00}^+(Q^2)$  have been plotted with respect to  $Q^2$  in (a) and (b), respectively, for both  $\rho$  and  $J/\psi$ -mesons. The helicity-flip matrix element with one unit  $G_{0+}^+(Q^2)$  and two units  $G_{-+}^+(Q^2)$  of helicity-flip has been plotted in (c) and (d), respectively, for both  $\rho$  and  $J/\psi$ -mesons.

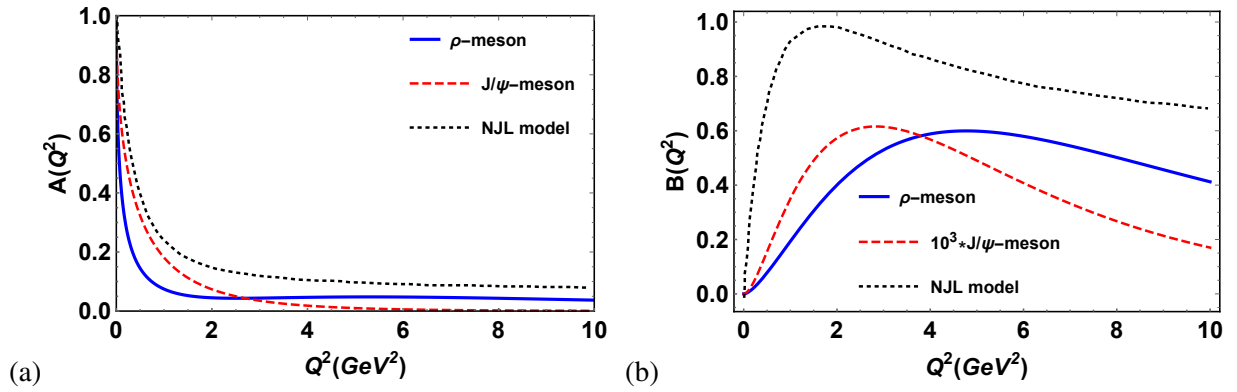


FIG. 12: (Color online) The  $A(Q^2)$  and  $B(Q^2)$  structure function of light  $\rho$  and heavy  $J/\psi$  vector meson along with comparison with NJL model.

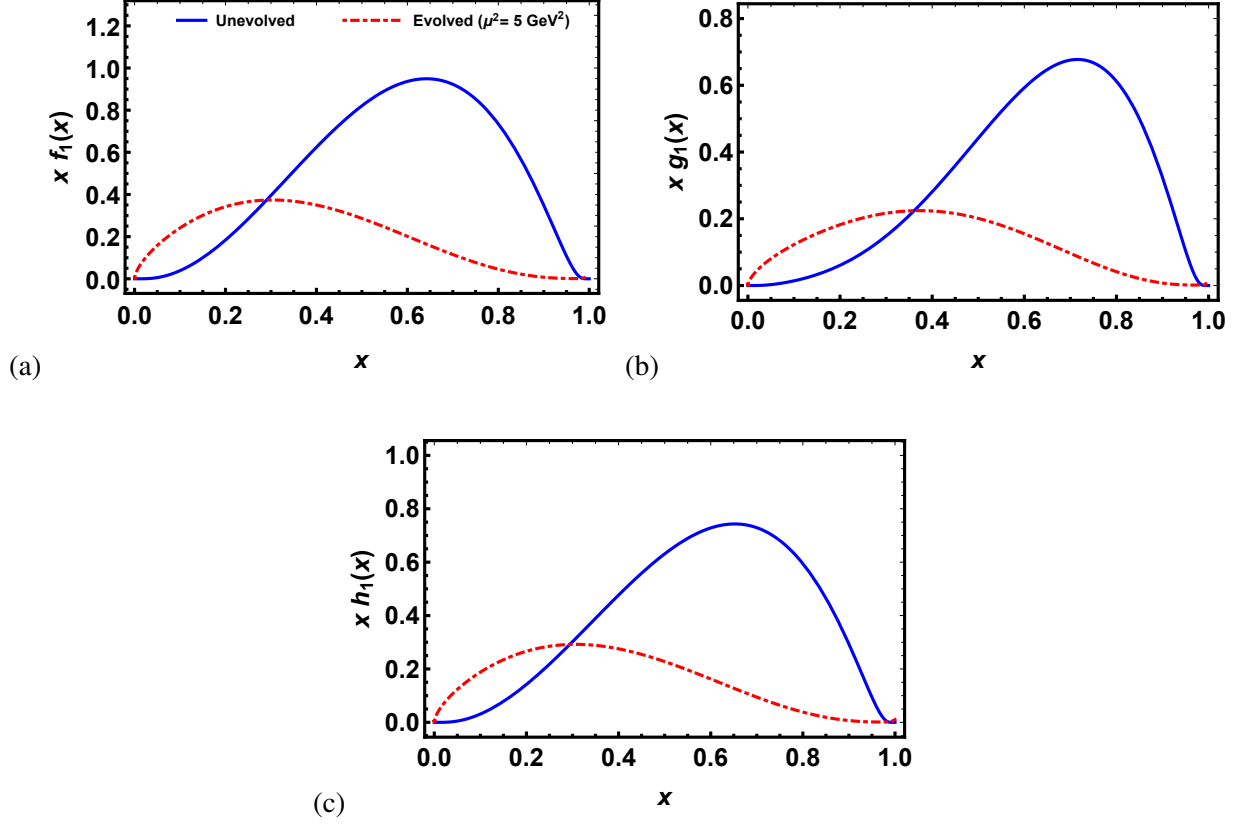


FIG. 13: (Color online) The unpolarized  $x f_1(x)$ , helicity  $x g_1(x)$ , and transversity polarized  $x h_1(x)$  quark PDFs have been plotted with respect to longitudinal momentum fraction  $x$  for light  $\rho$ -meson at model scale  $\mu_0^2 = 0.19 \text{ GeV}^2$  (blue solid line) and at scale  $\mu^2 = 5 \text{ GeV}^2$  (red dot dashed line) in (a), (b) and (c), respectively.

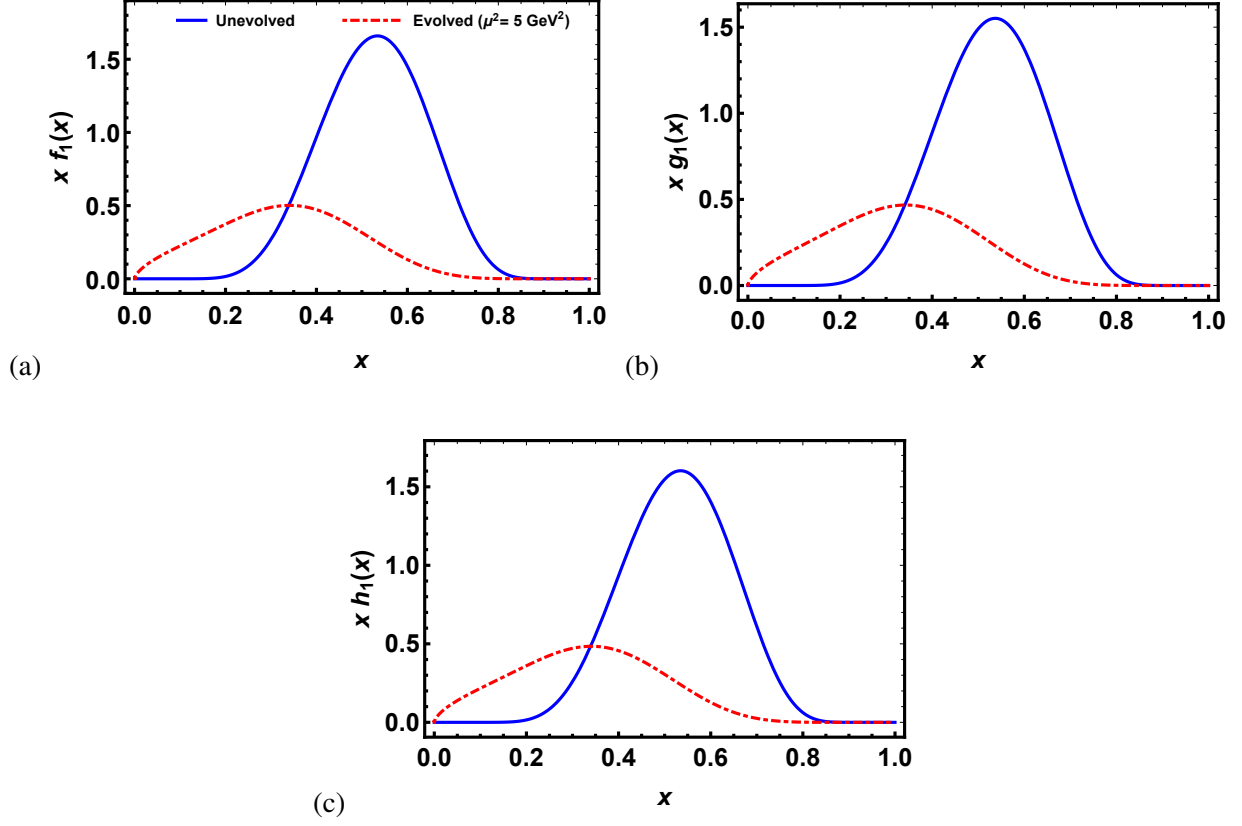


FIG. 14: (Color online) The unpolarized  $x f_1(x)$ , helicity  $x g_1(x)$ , and transversity polarized  $x h_1(x)$  quark PDFs have been plotted with respect to longitudinal momentum fraction  $x$  for heavy  $J/\psi$ -meson at model scale  $\mu_0^2 = 0.19 \text{ GeV}^2$  (blue solid line) and at scale  $\mu^2 = 5 \text{ GeV}^2$  (red dot dashed line) in (a), (b) and (c), respectively.

## V. CONCLUSION

In this work, we have evaluated the unpolarized quark generalized parton distributions (GPDs) of spin-1 vector  $\rho$  and  $J/\psi$  mesons at zero skewness, using the light-cone quark model (LCQM). We have employed the Brodsky-Huang-Lepage (BHL) prescription as the momentum space wave function, and the spin part of the wave function is obtained from the Melosh-Wigner rotation.

For spin-1 vector mesons, the unpolarized quark GPDs have been calculated using the correlator  $V_{S'_z, S_z}$ , which is an overlap of the initial and final state of the light-front wave function. Out of five unpolarized GPDs,  $H_4(x, 0, -\Delta_\perp^2)$  comes out to be zero. We have observed the three-dimensional behavior of the quark GPDs  $H_{1,2,3}(x, 0, -\Delta_\perp^2)$  with transverse momentum transferred and longitudinal momentum fraction. The GPDs of  $J/\psi$  mesons exhibit a sharper peak in  $x$  as compared to that in  $\rho$  mesons which can be attributed to the active quark carrying more momentum at lower  $x$  for the case of  $\rho$  mesons. Further, a symmetric distribution of  $H_1(x, 0, -\Delta_\perp^2)$ , as a function of  $x$  and  $\Delta_\perp^2$  along with a contribution of superpositioned S, P and D-waves, has been observed for both the vector mesons which is due to identical quark content. On the other hand, the distribution  $H_3(x, 0, -\Delta_\perp^2)$  has a contribution of D-wave and  $H_2(x, 0, -\Delta_\perp^2)$  has a contribution from S and P-wave. The behavior of these unpolarized quark GPDs has also been studied at finite values of  $x$  and  $\Delta_\perp^2$ . Additionally, we have examined the unpolarized quark GPDs in impact parameter space which is accomplished by taking the GPD's Fourier transform in momentum space.

In light of the recent progress, the electromagnetic form factors have also been extracted from the respective GPDs and have been further used to calculate the charge  $G_C(Q^2)$ , magnetic  $G_M(Q^2)$  and quadrupole  $G_Q(Q^2)$  form factors for both  $\rho$  and  $J/\psi$  mesons. Our results show a similar trend when compared with the lattice stimulation and other theoretical model results. Subsequently, physical observables such as the charge radii, magnetic moment, and quadrupole moment for both the vector mesons have also been computed and compared with the available data. We have also predicted the  $A(Q^2)$  and  $B(Q^2)$  structure functions for the Rosenbluth cross section in terms of charge, magnetic, and quadrupole form factors. Furthermore, we have also evaluated the four parton distribution functions (PDFs), namely, unpolarized  $f_1(x)$ , helicity  $g_1(x)$ , transversity  $h_1(x)$  and tensor  $f_{1LL}(x)$  PDFs of  $\rho$  and  $J/\psi$  mesons in LCQM at leading twist. Additionally, we have also evolved our PDFs from our model scale to higher scale  $\mu^2$  for both the vector mesons. This study may be significant to understand the  $\rho$ -meson lepton production [44, 90–92],  $\gamma\gamma^* \rightarrow \rho\rho$  [93] process as well as the results from the future Electron-Ion Collider (EIC) experiments [94, 95].

## VI. ACKNOWLEDGEMENT

H.D. would like to thank the Science and Engineering Research Board, Anusandhan-National Research Foundation, Government of India under the scheme SERB-POWER Fellowship (Ref No. SPF/2023/000116) for financial support.

## VII. APPENDIX

The explicit form of quark PDFs (by considering  $m_q = m_{\bar{q}} = m$ ) can be expressed as

$$f_1(x) = \int \frac{d^2\mathbf{k}_\perp}{3(16\pi^3)} \left[ ((\mathbf{k}_\perp(1-2x)M_{q\bar{q}})^2 + (2\mathbf{k}_\perp^2 + (M_{q\bar{q}} + 2m)m)^2) + \right. \\ \left. + 2((\mathbf{k}_\perp^2(M_{q\bar{q}} + 2m)m) + \mathbf{k}_\perp^2(xM_{q\bar{q}} + m) + (-\mathbf{k}_\perp(1-x)M_{q\bar{q}} + m)^2 + \mathbf{k}_\perp^4) \right] \frac{|\psi_{q\bar{q}}(x, \mathbf{k}_\perp)|^2}{\omega_{q\bar{q}}^2}, \quad (59)$$

$$g_1(x) = \int \frac{d^2\mathbf{k}_\perp}{16\pi^3} \left[ (\mathbf{k}_\perp^2 + (M_{q\bar{q}} + 2m)m)^2 + (\mathbf{k}_\perp(xM_{q\bar{q}} + m))^2 \right. \\ \left. - \mathbf{k}_\perp^4 - (\mathbf{k}_\perp((1-x)M_{q\bar{q}} + m))^2 \right] \frac{|\psi_{q\bar{q}}(x, \mathbf{k}_\perp)|^2}{\omega_{q\bar{q}}^2}, \quad (60)$$

$$h_1(x) = \int \frac{d^2\mathbf{k}_\perp}{16\pi^3} \left[ ((2\mathbf{k}_\perp^2 + (M_{q\bar{q}} + 2m)m)(\mathbf{k}_\perp^2 + (M_{q\bar{q}} + 2m)m)) \right. \\ \left. + (\frac{1}{2}\mathbf{k}_\perp^2(1-2x)(1-x)M_{q\bar{q}}^2) - (\frac{1}{2}(xM_{q\bar{q}} + m)(1-2x)M_{q\bar{q}}) \right] \frac{|\psi_{q\bar{q}}(x, \mathbf{k}_\perp)|^2}{\omega_{q\bar{q}}^2}, \quad (61)$$

$$f_{1ll} = 0. \quad (62)$$

## VIII. REFERENCE

- 
- [1] M. K. Volkov and A. E. Radzhabov, The Nambu-Jona-Lasinio model and its development, Phys. Usp. **49**, 551 (2006), arXiv:hep-ph/0508263.
  - [2] B. A. Arbuzov, M. K. Volkov, and I. V. Zaitsev, NJL model derived from QCD, Int. J. Mod. Phys. A **21**, 5721 (2006), arXiv:hep-ph/0604051.
  - [3] Y. Ninomiya, W. Bentz, and I. C. Cloët, Dressed Quark Mass Dependence of Pion and Kaon Form Factors, Phys. Rev. C **91**, 025202 (2015), arXiv:1406.7212 [nucl-th].

- [4] V. M. Belyaev and M. B. Johnson, Pion light cone wave functions and light front quark model, Phys. Lett. B **423**, 379 (1998), arXiv:hep-ph/9707329.
- [5] H.-M. Choi, H.-Y. Ryu, and C.-R. Ji, Spacelike and timelike form factors for the  $(\pi^0, \eta, \eta') \rightarrow \gamma^* \gamma$  transitions in the light-front quark model, Phys. Rev. D **96**, 056008 (2017), arXiv:1708.00736 [hep-ph].
- [6] A. Yadav, S. Puhan, and H. Dahiya, Radiative Transitions for the Ground and Excited Charmonia States, (2025), arXiv:2504.14864 [hep-ph].
- [7] S. J. Brodsky, G. F. de Teramond, H. G. Dosch, and J. Erlich, Light-Front Holographic QCD and Emerging Confinement, Phys. Rept. **584**, 1 (2015), arXiv:1407.8131 [hep-ph].
- [8] G. F. de Teramond and S. J. Brodsky, Light-Front Holography: A First Approximation to QCD, Phys. Rev. Lett. **102**, 081601 (2009), arXiv:0809.4899 [hep-ph].
- [9] A. Bacchetta, F. G. Celiberto, M. Radici, and P. Tael, A spectator-model way to transverse-momentum-dependent gluon distribution functions, SciPost Phys. Proc. **8**, 040 (2022), arXiv:2107.13446 [hep-ph].
- [10] C. Lorc  , B. Pasquini, and P. Schweitzer, Transverse pion structure beyond leading twist in constituent models, Eur. Phys. J. C **76**, 415 (2016), arXiv:1605.00815 [hep-ph].
- [11] N. Strodthoff, B.-J. Schaefer, and L. von Smekal, Quark-meson-diquark model for two-color QCD, Phys. Rev. D **85**, 074007 (2012), arXiv:1112.5401 [hep-ph].
- [12] T. Maji and D. Chakrabarti, Light front quark-diquark model for the nucleons, Phys. Rev. D **94**, 094020 (2016), arXiv:1608.07776 [hep-ph].
- [13] A. I. Signal and F. G. Cao, Transverse momentum and transverse momentum distributions in the MIT bag model, Phys. Lett. B **826**, 136898 (2022), arXiv:2108.12116 [hep-ph].
- [14] K. Johnson, The M.I.T. Bag Model, Acta Phys. Polon. B **6**, 865 (1975).
- [15] J.-L. Zhang, Kaon GTMDs in the Dyson-Schwinger equations using contact interaction, (2024), arXiv:2409.04105 [hep-ph].
- [16] J.-L. Zhang, Z.-F. Cui, J. Ping, and C. D. Roberts, Contact interaction analysis of pion GTMDs, Eur. Phys. J. C **81**, 6 (2021), arXiv:2009.11384 [hep-ph].
- [17] H.-W. Lin *et al.*, Parton distributions and lattice QCD calculations: a community white paper, Prog. Part. Nucl. Phys. **100**, 107 (2018), arXiv:1711.07916 [hep-ph].
- [18] M. J. Savage, Nuclear Physics from Lattice QCD, Prog. Part. Nucl. Phys. **67**, 140 (2012), arXiv:1110.5943 [nucl-th].

- [19] L. Y. Glozman, C. B. Lang, and M. Limmer, Angular momentum content of the rho-meson in lattice QCD, Phys. Rev. Lett. **103**, 121601 (2009), arXiv:0905.0811 [hep-lat].
- [20] S. Puhan, S. Sharma, N. Kumar, and H. Dahiya, Understanding the Valence Quark Structure of the Pion through GTMDs, (2025), arXiv:2504.14982 [hep-ph].
- [21] M. G. Echevarria, A. Idilbi, K. Kanazawa, C. Lorcé, A. Metz, B. Pasquini, and M. Schlegel, Proper definition and evolution of generalized transverse momentum dependent distributions, Phys. Lett. B **759**, 336 (2016), arXiv:1602.06953 [hep-ph].
- [22] S. Meissner, A. Metz, and M. Schlegel, Generalized parton correlation functions for a spin-1/2 hadron, JHEP **08**, 056, arXiv:0906.5323 [hep-ph].
- [23] S. Meissner, A. Metz, M. Schlegel, and K. Goeke, Generalized parton correlation functions for a spin-0 hadron, JHEP **08**, 038, arXiv:0805.3165 [hep-ph].
- [24] M. Diehl, Generalized parton distributions, Phys. Rept. **388**, 41 (2003), arXiv:hep-ph/0307382.
- [25] J. M. M. Chavez, V. Bertone, F. De Soto Borrero, M. Defurne, C. Mezrag, H. Moutarde, J. Rodríguez-Quintero, and J. Segovia, Pion generalized parton distributions: A path toward phenomenology, Phys. Rev. D **105**, 094012 (2022), arXiv:2110.06052 [hep-ph].
- [26] W. Broniowski, V. Shastry, and E. Ruiz Arriola, Off-shell generalized parton distributions and form factors of the pion, Phys. Lett. B **840**, 137872 (2023), arXiv:2211.11067 [hep-ph].
- [27] M. Guidal, M. V. Polyakov, A. V. Radyushkin, and M. Vanderhaeghen, Nucleon form-factors from generalized parton distributions, Phys. Rev. D **72**, 054013 (2005), arXiv:hep-ph/0410251.
- [28] M. Diehl, Introduction to GPDs and TMDs, Eur. Phys. J. A **52**, 149 (2016), arXiv:1512.01328 [hep-ph].
- [29] R. Angeles-Martinez *et al.*, Transverse Momentum Dependent (TMD) parton distribution functions: status and prospects, Acta Phys. Polon. B **46**, 2501 (2015), arXiv:1507.05267 [hep-ph].
- [30] B. Pasquini, S. Cazzaniga, and S. Boffi, Transverse momentum dependent parton distributions in a light-cone quark model, Phys. Rev. D **78**, 034025 (2008), arXiv:0806.2298 [hep-ph].
- [31] S. Puhan and H. Dahiya, Leading twist T-even TMDs for the spin-1 heavy vector mesons, Phys. Rev. D **109**, 034005 (2024), arXiv:2310.03465 [hep-ph].
- [32] J. C. Collins and D. E. Soper, Parton Distribution and Decay Functions, Nucl. Phys. B **194**, 445 (1982).
- [33] A. D. Martin, R. G. Roberts, W. J. Stirling, and R. S. Thorne, Parton distributions: A New global analysis, Eur. Phys. J. C **4**, 463 (1998), arXiv:hep-ph/9803445.



- [34] M. Gluck, E. Reya, and A. Vogt, Dynamical parton distributions of the proton and small  $x$  physics, *Z. Phys. C* **67**, 433 (1995).
- [35] A. Freese and I. C. Cloët, Quark spin and orbital angular momentum from proton generalized parton distributions, *Phys. Rev. C* **103**, 045204 (2021), arXiv:2005.10286 [nucl-th].
- [36] M. Guidal, H. Moutarde, and M. Vanderhaeghen, Generalized Parton Distributions in the valence region from Deeply Virtual Compton Scattering, *Rept. Prog. Phys.* **76**, 066202 (2013), arXiv:1303.6600 [hep-ph].
- [37] X.-D. Ji, Deeply virtual Compton scattering, *Phys. Rev. D* **55**, 7114 (1997), arXiv:hep-ph/9609381.
- [38] G. Xie, W. Kou, Q. Fu, Z. Ye, and X. Chen, Deeply virtual compton scattering at future electron-ion colliders, *Eur. Phys. J. C* **83**, 900 (2023), arXiv:2306.02357 [hep-ph].
- [39] L. Favart, M. Guidal, T. Horn, and P. Kroll, Deeply Virtual Meson Production on the nucleon, *Eur. Phys. J. A* **52**, 158 (2016), arXiv:1511.04535 [hep-ph].
- [40] S. Alekhin, Parton distributions from deep inelastic scattering data, *Phys. Rev. D* **68**, 014002 (2003), arXiv:hep-ph/0211096.
- [41] S. Puan, S. Sharma, N. Kaur, N. Kumar, and H. Dahiya, T-even TMDs for the spin-0 pseudo-scalar mesons upto twist-4 using light-front formalism, *JHEP* **02**, 075, arXiv:2310.03464 [hep-ph].
- [42] W. Qian and B.-Q. Ma, Vector meson omega-phi mixing and their form factors in light-cone quark model, *Phys. Rev. D* **78**, 074002 (2008), arXiv:0809.4411 [hep-ph].
- [43] S. J. Brodsky, M. Diehl, and D. S. Hwang, Light cone wave function representation of deeply virtual Compton scattering, *Nucl. Phys. B* **596**, 99 (2001), arXiv:hep-ph/0009254.
- [44] F. Cano and B. Pire, Deep electroproduction of photons and mesons on the deuteron, *Eur. Phys. J. A* **19**, 423 (2004), arXiv:hep-ph/0307231.
- [45] J.-L. Zhang, G.-Z. Kang, and J.-L. Ping,  $\rho$  meson generalized parton distributions in the Nambu–Jona-Lasinio model, *Phys. Rev. D* **105**, 094015 (2022), arXiv:2204.14032 [hep-ph].
- [46] B.-D. Sun and Y.-B. Dong, Polarized generalized parton distributions and structure functions of the  $\rho$  meson, *Phys. Rev. D* **99**, 016023 (2019), arXiv:1811.00666 [hep-ph].
- [47] N. Kumar, Transverse densities and generalized parton distributions of the  $\rho$  meson in the light front quark model, *Phys. Rev. D* **99**, 014039 (2019), arXiv:1901.02836 [hep-ph].
- [48] L. Adhikari, Y. Li, M. Li, and J. P. Vary, Form factors and generalized parton distributions of heavy quarkonia in basis light front quantization, *Phys. Rev. C* **99**, 035208 (2019), arXiv:1809.06475 [hep-ph].

- [49] C. Shi, J. Li, P.-L. Yin, and W. Jia, Unpolarized generalized parton distributions of light and heavy vector mesons, *Phys. Rev. D* **107**, 074009 (2023), arXiv:2302.02388 [hep-ph].
- [50] B.-D. Sun and Y.-B. Dong,  $\rho$  meson unpolarized generalized parton distributions with a light-front constituent quark model, *Phys. Rev. D* **96**, 036019 (2017), arXiv:1707.03972 [hep-ph].
- [51] S. Puhan, N. Kumar, and H. Dahiya, Spin-1 unpolarized GPDs in light front formalism, *DAE Symp. Nucl. Phys.* **68**, 825 (2025).
- [52] H.-M. Choi and C.-R. Ji, Electromagnetic structure of the rho meson in the light front quark model, *Phys. Rev. D* **70**, 053015 (2004), arXiv:hep-ph/0402114.
- [53] R. Hofstadter, Nuclear and nucleon scattering of high-energy electrons, *Ann. Rev. Nucl. Part. Sci.* **7**, 231 (1957).
- [54] V. A. Karmanov, On ambiguities of the spin-1 electromagnetic form-factors in light front dynamics, *Nucl. Phys. A* **608**, 316 (1996).
- [55] P. L. Chung, F. Coester, and W. N. Polyzou, Charge Form-Factors of Quark Model Pions, *Phys. Lett. B* **205**, 545 (1988).
- [56] S. J. Brodsky and J. R. Hiller, Universal properties of the electromagnetic interactions of spin one systems, *Phys. Rev. D* **46**, 2141 (1992).
- [57] L. L. Frankfurt, M. Strikman, and T. Frederico, Deuteron form-factors in the light cone quantum mechanics 'good' component approach, *Phys. Rev. C* **48**, 2182 (1993).
- [58] J. P. B. C. De Melo, Unambiguous Extraction of the Electromagnetic Form Factors for Spin-1 Particles on the Light-Front, *Phys. Lett. B* **788**, 152 (2019), arXiv:1810.11478 [hep-ph].
- [59] M. Allahverdiyeva and S. Mamedov, Vector meson gravitational form factors and generalized parton distributions at finite temperature within the soft-wall AdS/QCD model, *Eur. Phys. J. C* **83**, 447 (2023), arXiv:2302.03383 [hep-ph].
- [60] M. Gurtler *et al.* (QCDSF), Vector meson electromagnetic form factors, *PoS LATTICE2008*, 051 (2008).
- [61] C. J. Shultz, J. J. Dudek, and R. G. Edwards, Excited meson radiative transitions from lattice QCD using variationally optimized operators, *Phys. Rev. D* **91**, 114501 (2015), arXiv:1501.07457 [hep-lat].
- [62] A. Bacchetta and P. J. Mulders, Deep inelastic leptonproduction of spin-one hadrons, *Phys. Rev. D* **62**, 114004 (2000), arXiv:hep-ph/0007120.
- [63] G. P. Lepage and S. J. Brodsky, Exclusive Processes in Perturbative Quantum Chromodynamics, *Phys. Rev. D* **22**, 2157 (1980).

- [64] H. M. Choi and C.-R. Ji, Light cone quark model predictions for radiative meson decays, Nucl. Phys. A **618**, 291 (1997).
- [65] S. J. Brodsky, H.-C. Pauli, and S. S. Pinsky, Quantum chromodynamics and other field theories on the light cone, Phys. Rept. **301**, 299 (1998), arXiv:hep-ph/9705477.
- [66] B. Pasquini, S. Rodini, and S. Venturini (MAP (Multi-dimensional Analyses of Partonic distributions)), Valence quark, sea, and gluon content of the pion from the parton distribution functions and the electromagnetic form factor, Phys. Rev. D **107**, 114023 (2023), arXiv:2303.01789 [hep-ph].
- [67] C. Shi, J. Li, M. Li, X. Chen, and W. Jia, Transverse momentum distributions of valence quarks in light and heavy vector mesons, Phys. Rev. D **106**, 014026 (2022), arXiv:2205.02757 [hep-ph].
- [68] B.-W. Xiao, X. Qian, and B.-Q. Ma, The Kaon form-factor in the light cone quark model, Eur. Phys. J. A **15**, 523 (2002), arXiv:hep-ph/0209138.
- [69] S. Kaur, C. Mondal, and H. Dahiya, Light-front holographic  $\rho$ -meson distributions in the momentum space, JHEP **01**, 136, arXiv:2009.04288 [hep-ph].
- [70] S. Kaur, N. Kumar, J. Lan, C. Mondal, and H. Dahiya, Tomography of light mesons in the light-cone quark model, Phys. Rev. D **102**, 014021 (2020), arXiv:2002.01199 [hep-ph].
- [71] E. R. Berger, F. Cano, M. Diehl, and B. Pire, Generalized parton distributions in the deuteron, Phys. Rev. Lett. **87**, 142302 (2001), arXiv:hep-ph/0106192.
- [72] B. G. Lasscock, J. Hedditch, D. B. Leinweber, and A. G. Williams, Vector meson electromagnetic form factors, PoS LAT2006, 114 (2006), arXiv:hep-lat/0611029.
- [73] J.-L. Zhang,  $\rho$  meson form factors and parton distribution functions in impact parameter space\*, Chin. Phys. C **49**, 043104 (2025), arXiv:2409.19525 [hep-ph].
- [74] R. J. Hernández-Pinto, L. X. Gutiérrez-Guerrero, M. A. Bedolla, and A. Bashir, Electric, magnetic, and quadrupole form factors and charge radii of vector mesons: From light to heavy sectors in a contact interaction, Phys. Rev. D **110**, 114015 (2024), arXiv:2410.23813 [hep-ph].
- [75] M. S. Bhagwat and P. Maris, Vector meson form factors and their quark-mass dependence, Phys. Rev. C **77**, 025203 (2008), arXiv:nucl-th/0612069.
- [76] J. J. Dudek, R. G. Edwards, and D. G. Richards, Radiative transitions in charmonium from lattice QCD, Phys. Rev. D **73**, 074507 (2006), arXiv:hep-ph/0601137.
- [77] Y.-L. Luan, X.-L. Chen, and W.-Z. Deng, Meson electro-magnetic form factors in an extended Nambu–Jona-Lasinio model including heavy quark flavors, Chin. Phys. C **39**, 113103 (2015), arXiv:1504.03799 [hep-ph].

- [78] B. Owen, W. Kamleh, D. Leinweber, B. Menadue, and S. Mahbub, Light Meson Form Factors at near Physical Masses, *Phys. Rev. D* **91**, 074503 (2015), arXiv:1501.02561 [hep-lat].
- [79] M. I. Haftel, L. Mathelitsch, and H. F. K. Zingl, Electron-deuteron tensor polarization and the two-nucleon force, *Phys. Rev. C* **22**, 1285 (1980).
- [80] S. Kumano and Q.-T. Song, Twist-2 relation and sum rule for tensor-polarized parton distribution functions of spin-1 hadrons, *JHEP* **09**, 141, arXiv:2106.15849 [hep-ph].
- [81] S. Hino and S. Kumano, Structure functions in the polarized Drell-Yan processes with spin 1/2 and spin 1 hadrons. 2. Parton model, *Phys. Rev. D* **60**, 054018 (1999), arXiv:hep-ph/9902258.
- [82] W. Cosyn, Y.-B. Dong, S. Kumano, and M. Sargsian, Tensor-polarized structure function  $b_1$  in standard convolution description of deuteron, *Phys. Rev. D* **95**, 074036 (2017), arXiv:1702.05337 [hep-ph].
- [83] M. Miyama and S. Kumano, Numerical solution of  $Q^{*2}$  evolution equations in a brute force method, *Comput. Phys. Commun.* **94**, 185 (1996), arXiv:hep-ph/9508246.
- [84] M. Hirai, S. Kumano, and M. Miyama, Numerical solution of  $Q^{*2}$  evolution equations for polarized structure functions, *Comput. Phys. Commun.* **108**, 38 (1998), arXiv:hep-ph/9707220.
- [85] M. Hirai, S. Kumano, and M. Miyama, Numerical solution of  $Q^{*2}$  evolution equation for the transversity distribution  $\Delta(T)q$ , *Comput. Phys. Commun.* **111**, 150 (1998), arXiv:hep-ph/9712410.
- [86] Y. Ninomiya, W. Bentz, and I. C. Cloët, Transverse-momentum-dependent quark distribution functions of spin-one targets: Formalism and covariant calculations, *Phys. Rev. C* **96**, 045206 (2017), arXiv:1707.03787 [nucl-th].
- [87] J.-L. Zhang and J. Wu,  $\rho$  meson transverse momentum-dependent parton distributions, *Eur. Phys. J. C* **85**, 13 (2025), arXiv:2408.13569 [hep-ph].
- [88] J. Lan, C. Mondal, M. Li, Y. Li, S. Tang, X. Zhao, and J. P. Vary, Parton Distribution Functions of Heavy Mesons on the Light Front, *Phys. Rev. D* **102**, 014020 (2020), arXiv:1911.11676 [nucl-th].
- [89] M. Li, Y. Li, G. Chen, T. Lappi, and J. P. Vary, Light-front wavefunctions of mesons by design, *Eur. Phys. J. C* **82**, 1045 (2022), arXiv:2111.07087 [hep-ph].
- [90] A. Airapetian *et al.* (HERMES), Ratios of helicity amplitudes for exclusive  $\rho^0$  electroproduction on transversely polarized protons, *Eur. Phys. J. C* **77**, 378 (2017), arXiv:1702.00345 [hep-ex].
- [91] L. Mankiewicz, G. Piller, and T. Weigl, Hard exclusive meson production and nonforward parton distributions, *Eur. Phys. J. C* **5**, 119 (1998), arXiv:hep-ph/9711227.

- [92] S. A. Morrow *et al.* (CLAS), Exclusive  $\rho^0$  electroproduction on the proton at CLAS, Eur. Phys. J. A **39**, 5 (2009), arXiv:0807.3834 [hep-ex].
- [93] I. V. Anikin, B. Pire, and O. V. Teryaev, On  $\gamma\gamma^*$  production of two  $\rho^0$  mesons, Phys. Rev. D **69**, 014018 (2004), arXiv:hep-ph/0307059.
- [94] D. Boer *et al.*, Gluons and the quark sea at high energies: Distributions, polarization, tomography, (2011), arXiv:1108.1713 [nucl-th].
- [95] R. Abdul Khalek *et al.*, Science Requirements and Detector Concepts for the Electron-Ion Collider: EIC Yellow Report, Nucl. Phys. A **1026**, 122447 (2022), arXiv:2103.05419 [physics.ins-det].